NMR
Applications

Structural information

1. ***Interproton distances :***

   $NOE \propto R^{-6}$

2. ***Dihedral angles :***

   J-coupling and Karplus equations

3. ***Chemical Shift Index (CSI) :***

   Chemical shift of H^{α}, C^{α}, C^{β}, *CO*

4. ***Hydrogen bonding :***

   Amide proton exchange rates

Resonance assignment strategies for small proteins

1. ***Spin system identification :***
   DQF-COSY and TOCSY experiments
2. ***Sequence-specific assignment :***
   NOESY experiment

For protein < 10 kDa, 2D homonuclear experiments may be sufficient for resolving overlapping NMR resonances.

DQF-COSY : Double-Quantum Filter-Correlation Spectroscopy

TOCSY : Total Correlation Spectroscopy

NOESY : Nuclear Overhauser Effect Spectroscopy

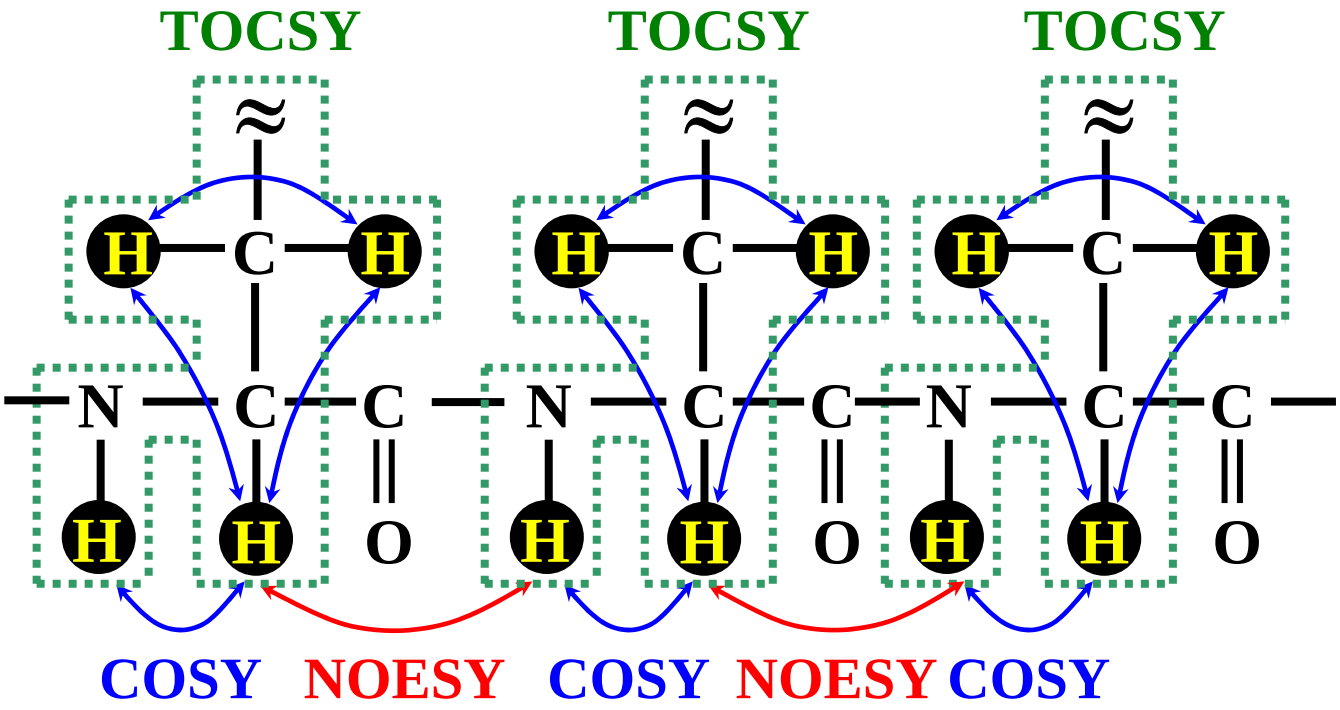
TOCSY
TOCSY
TOCSY
≈
H
C
H
N
C
C
H
H
O
COSY
NOESY
COSY
NOESY
COSY

Groups of Hydrogen Atoms in the Common Amino Acid Residues with similar Random Coil ^1H Chemical Shifts[a].

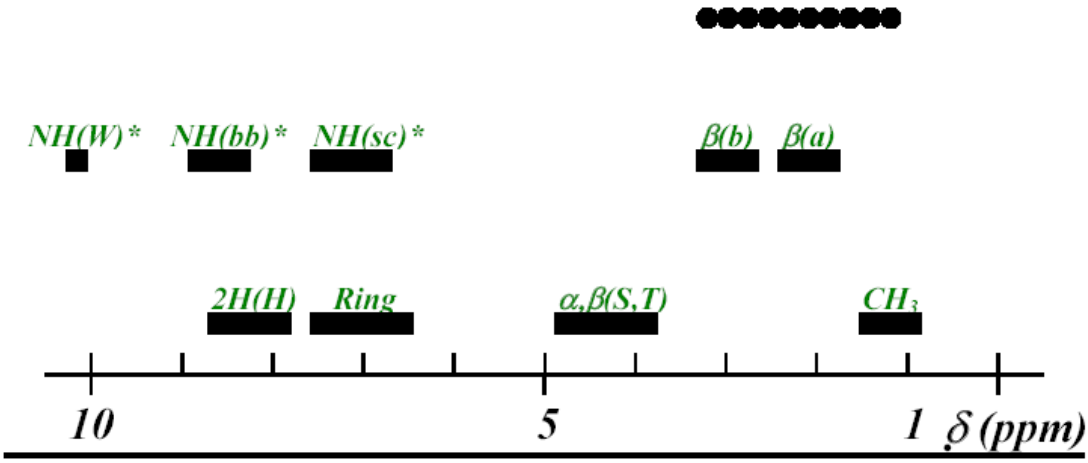

Code	(ppm)	Comments
CH_3	0.9-1.4	
β(a)	1.6-2.3	βH of V, I, L, E, Q, M, P, R, K
β(b)	2.7-3.3	βH of C, D, N, F, Y, H, W
●●●●●●●	1.2-3.3	Other aliphatic CH
α,β (S,T)	3.9-4.8	All αH, βH of S and T
Ring	6.5-7.7	Aromatic CH of F, Y, W; 4H of H
2H(H)	7.7-8.6	2H of H in the pH range 1-11
NH(sc)*	6.6-7.6	Side chain NH of N, Q, K, R
NH(bb)*	8.1-8.8	Backbone NH
NH(W)*	10.2	Indole NH of W

[a]In model peptides the labile protons (identified by *) are only observed in H_2O solution.
The singlet resonance of εCH_3 in Met is at 2.13 ppm.

CIEAKLTDTTTES (13-mer peptide)

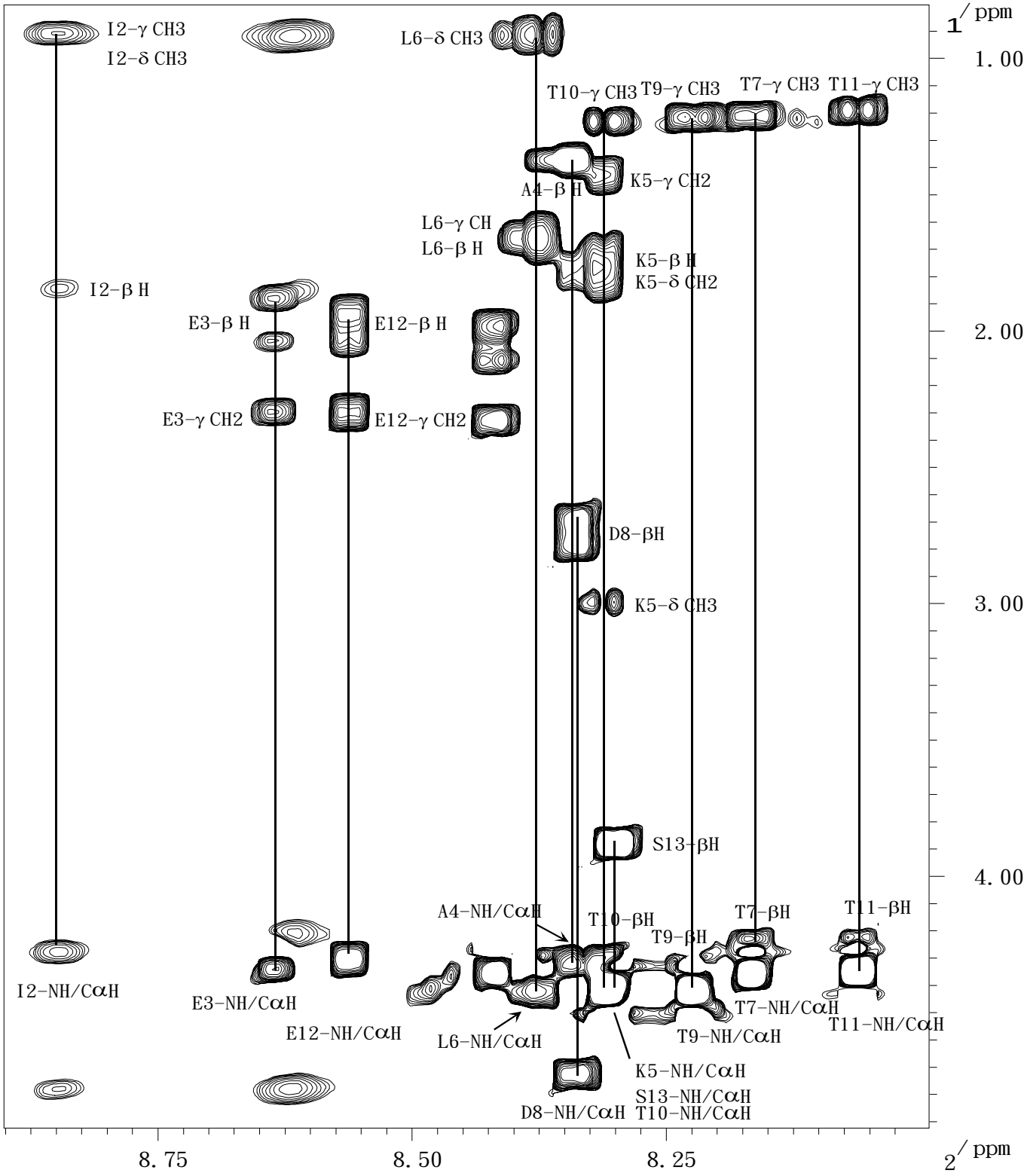

Fig 5-19 胜肽Den7 TOCSY光譜圖, pH 5.0的50mM phosphate buffer 300 μL及30 μL D2O,298K的條件下測得

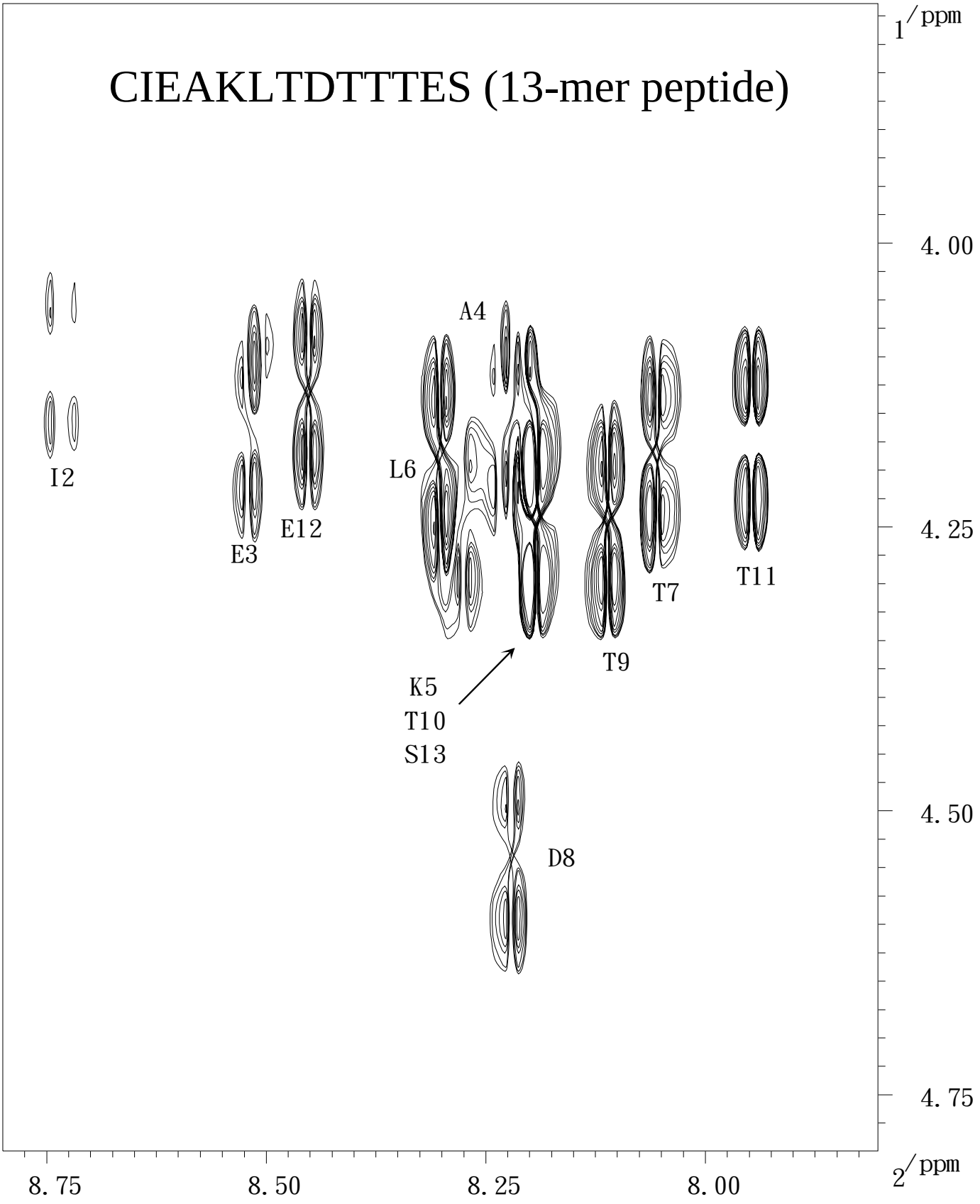

Fig 5-17 胜肽Den7 DQF-COSY光譜圖, pH 5.0的50mM phosphate buffer 300 μL及30 μL D2O,298K的條件下測得

CIEAKLTDTTTES (13-mer peptide)

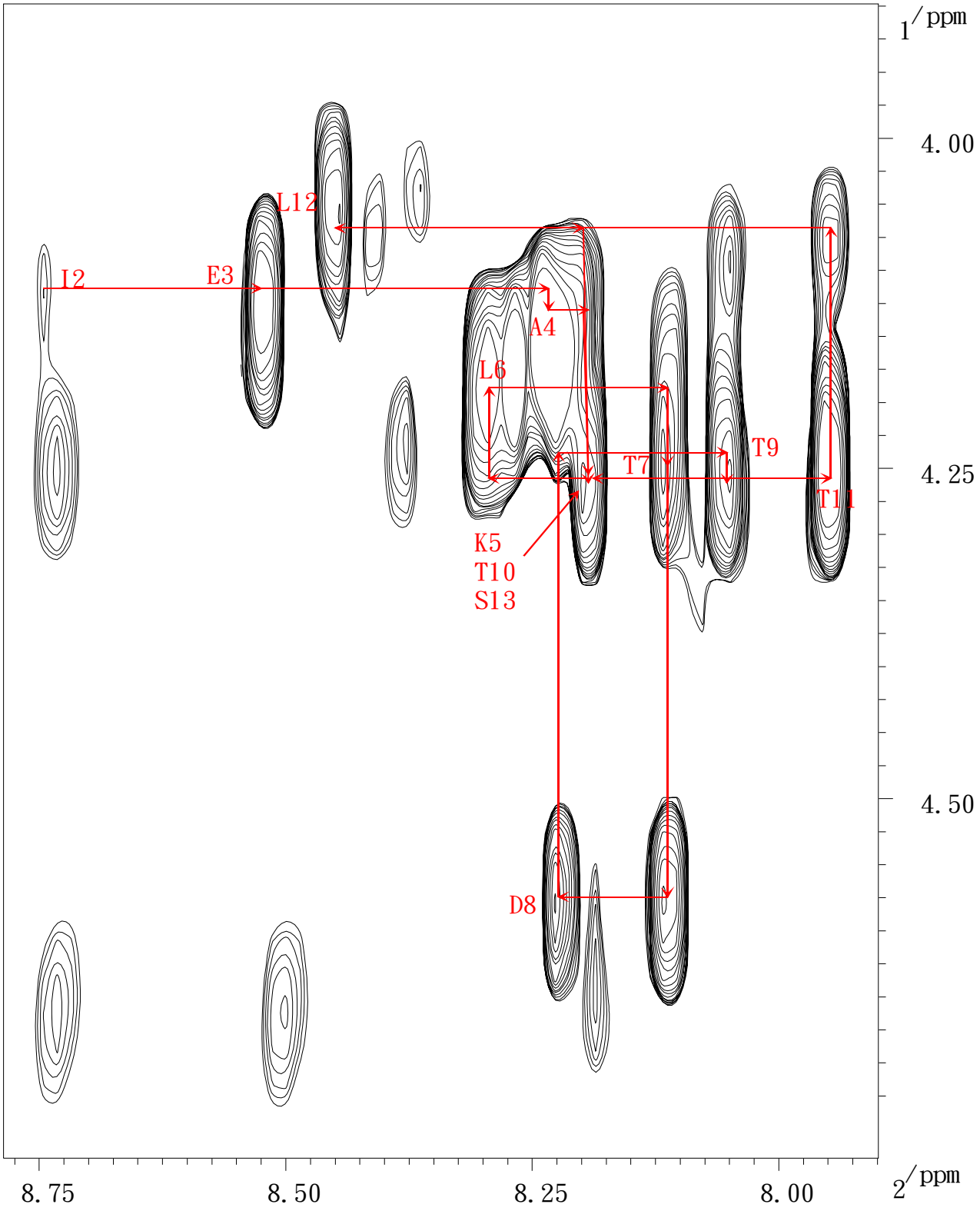

Fig 5-18 胜肽Den7 NOESY光譜圖, pH 5.0的50mM phosphate buffer 300 μL及30 μL D2O,298K,mixing time爲450ms的條件下測得

1D proton NMR spectra of I–2(1–172)

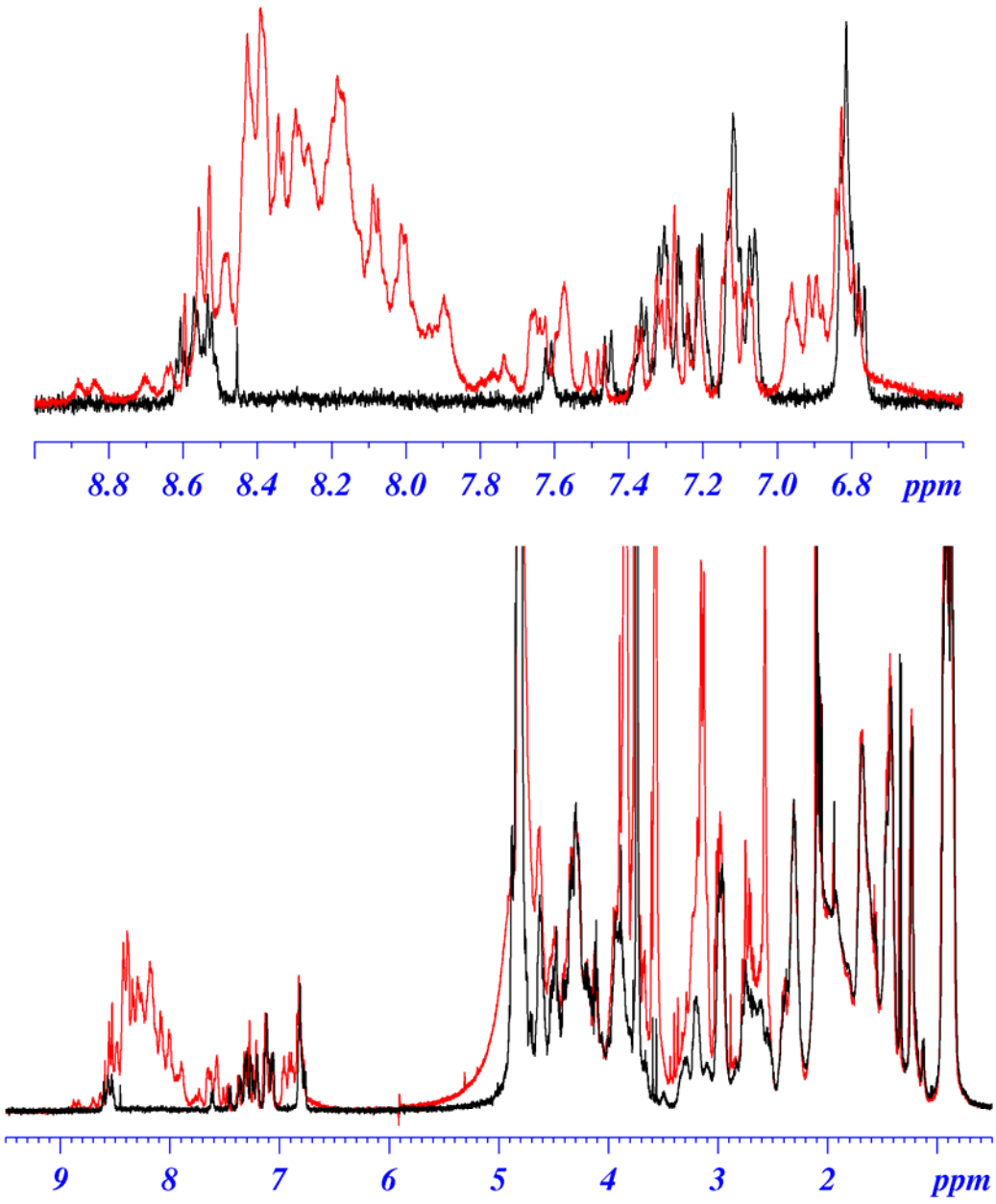

Determination of Macromolecular Structure by Multidimensional NMR Spectroscopy

Spin-spin coupling constants in peptides

Spin-spin coupling constants, like chemical shifts, depend on chemical environment and are therefore of great use in structure determination.

J-coupling constants

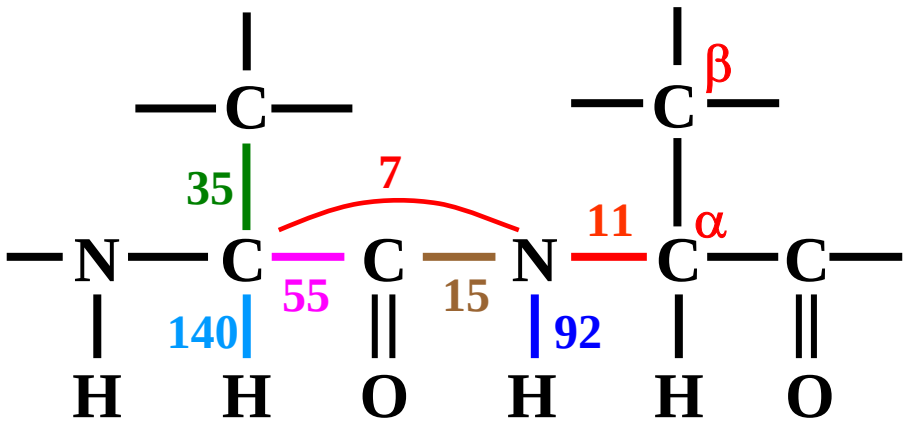

The flowchart of the protein structure determination from NMR data

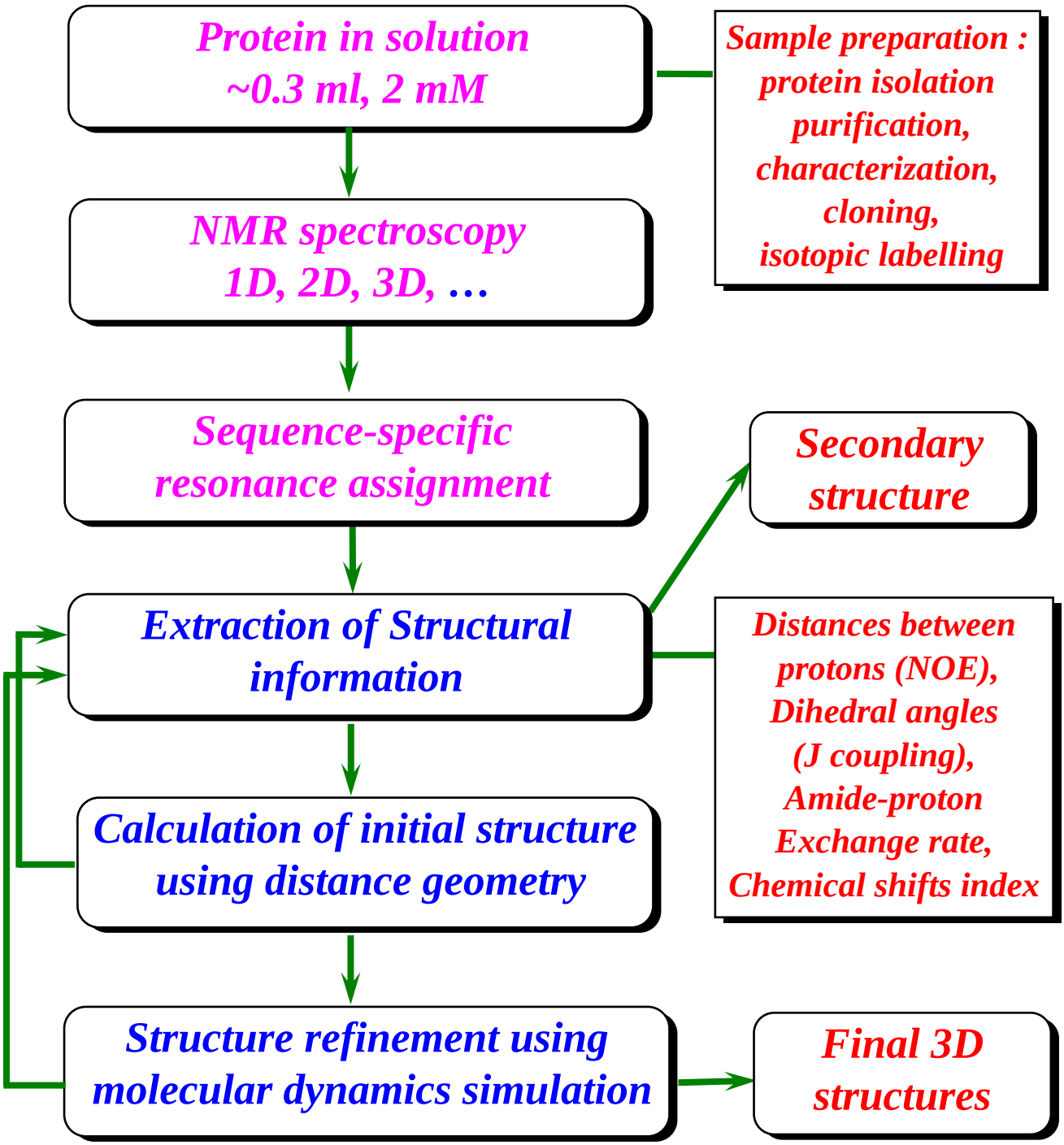

(a) HNCO : $H^N(i) \leftrightarrow N(i) \leftrightarrow C'(i-1)$

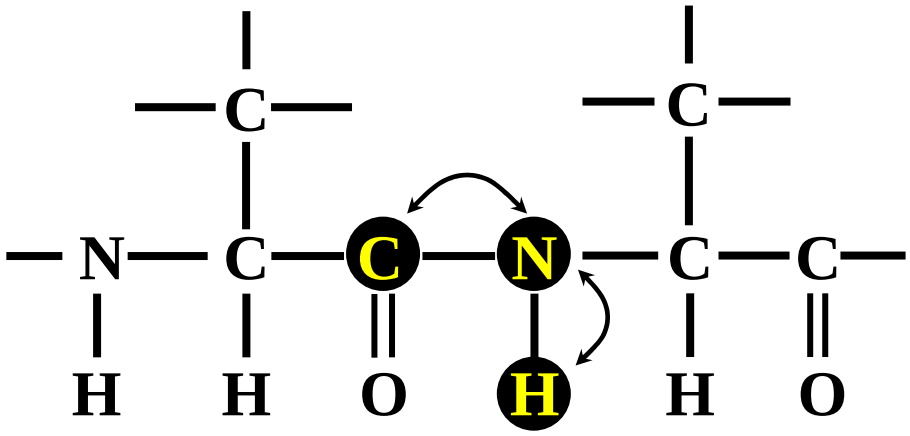

(b) HN(CA)CO : $H^N(i) \leftrightarrow N(i) \leftrightarrow C^{\alpha}(i) \leftrightarrow C'(i)$

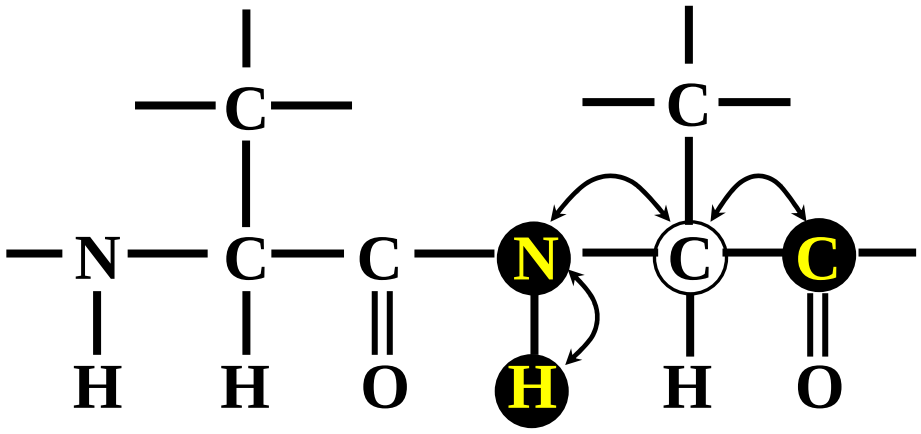

(c) HNCA : $H^N(i) \leftrightarrow N(i) \leftrightarrow C^\alpha(i-1)$, $C^\alpha(i)$

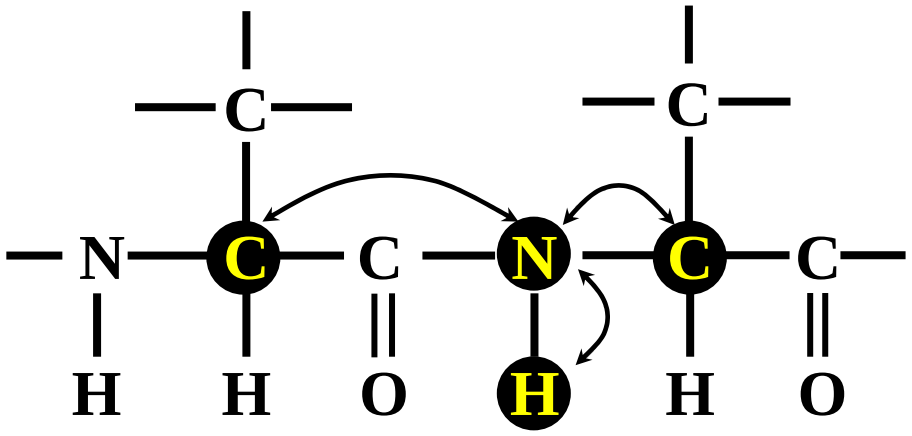

(d) HN(CO)CA : $H^N(i) \leftrightarrow N(i) \leftrightarrow C'(i-1) \leftrightarrow C^\alpha(i-1)$

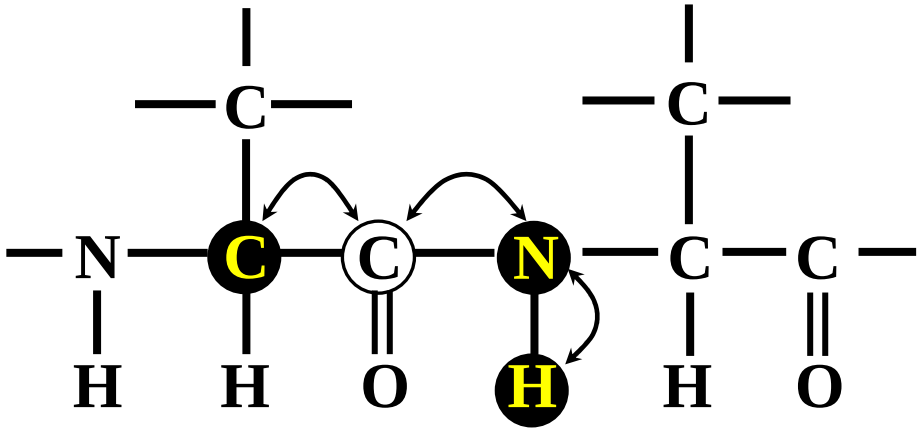

(e) HNCACB : $H^N(i) \leftrightarrow N(i)$ → $C^\alpha(i-1) \leftrightarrow C^\beta(i-1)$ and $C^\alpha(i) \leftrightarrow C^\beta(i)$

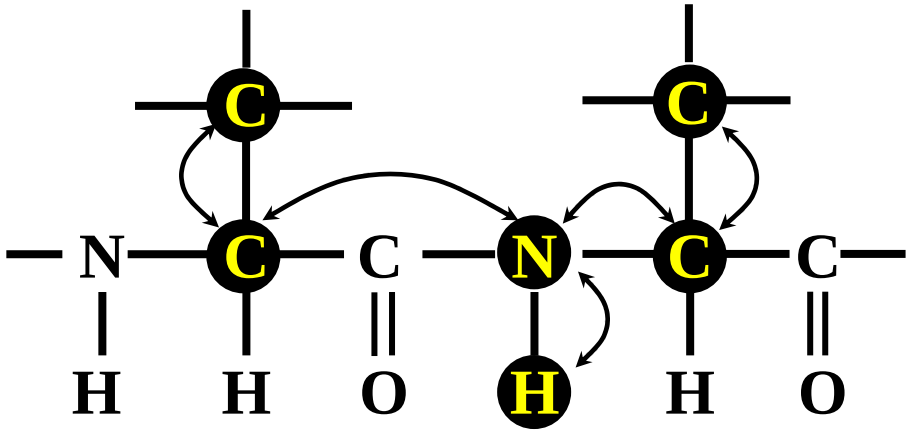

(f) CBCA(CO)NH :

$H^\alpha(i-1) \rightarrow C^\alpha(i-1) \rightarrow C'(i-1) \rightarrow N(i) \rightarrow H^N(i)$

$H^\beta(i-1) \rightarrow C^\beta(i-1)$

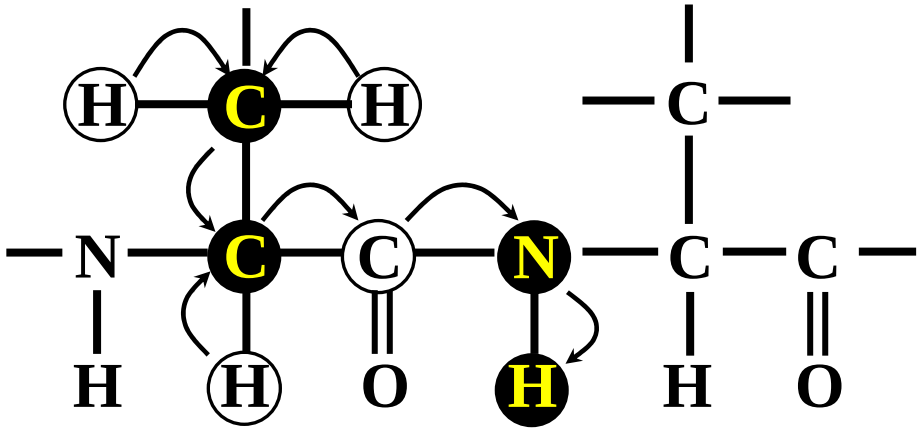

(g) HN(COCA)HA : $H^N(i) \longleftrightarrow N(i) \longleftrightarrow C'(i-1) \longleftrightarrow C^\alpha(i-1) \longleftrightarrow H^\alpha(i-1)$

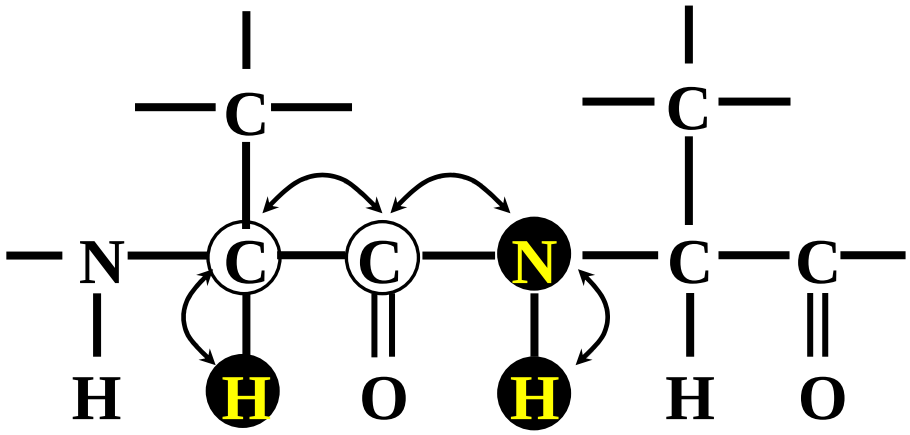

(h) HN(CA)HA : $H^N(i) \longleftrightarrow N(i) \longleftrightarrow C^\alpha(i) \longleftrightarrow H^\alpha(i)$

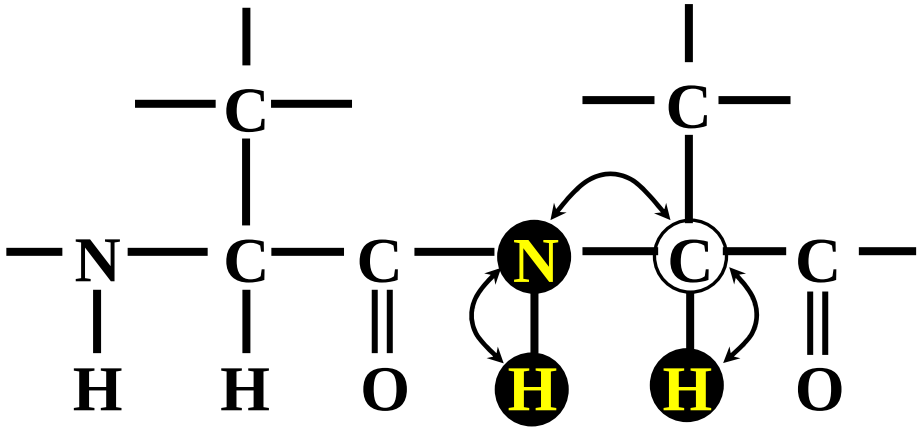

(i) TOCSY-HSQC : $H^{\gamma}(i) \longleftrightarrow H^{\beta}(i) \longleftrightarrow H^{\alpha}(i) \longleftrightarrow H^{N}(i) \longleftrightarrow N(i)$

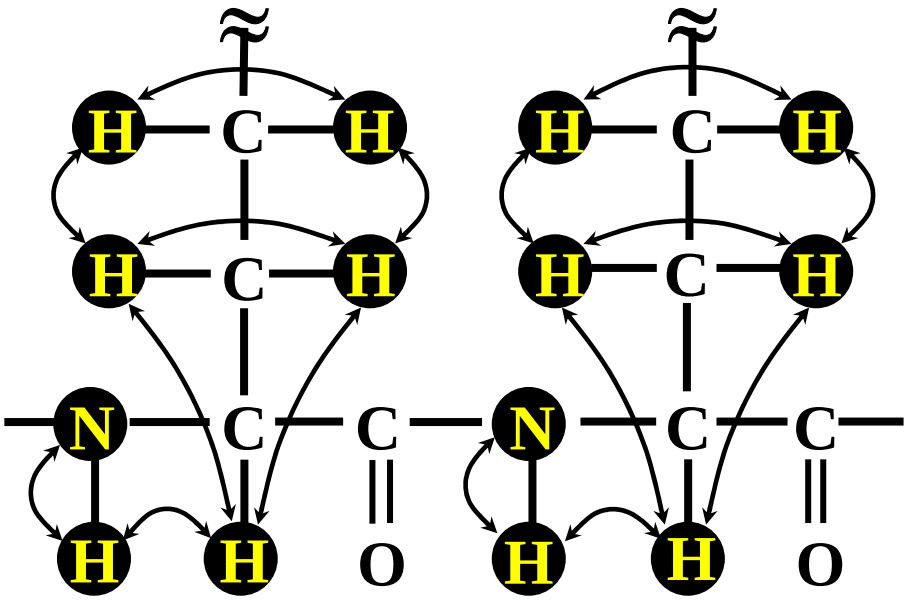

(j) HCCH-TOCSY : $H^{\alpha}(i) \longleftrightarrow C^{\alpha}(i)$, $H^{\beta}(i) \longleftrightarrow C^{\beta}(i)$, $H^{\gamma}(i) \longleftrightarrow C^{\gamma}(i)$

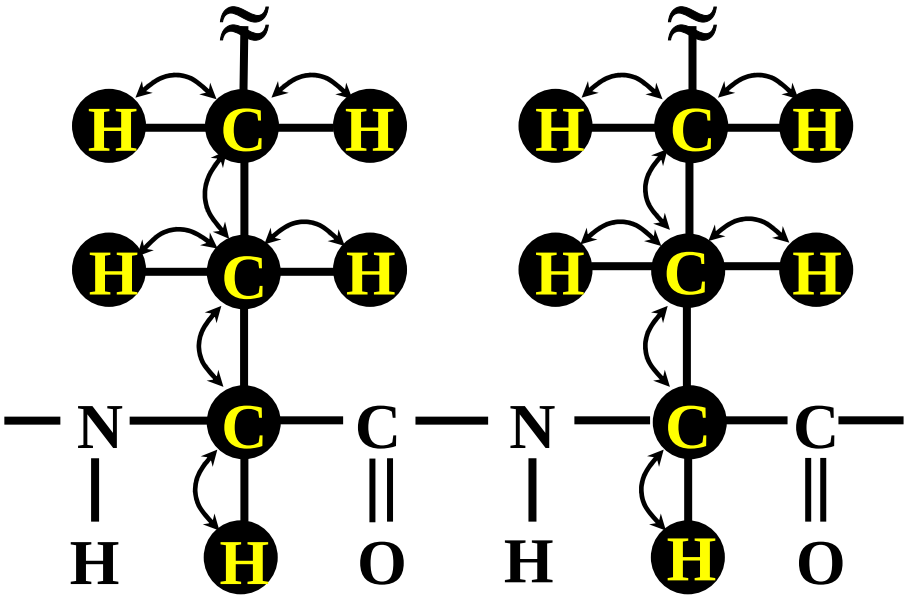

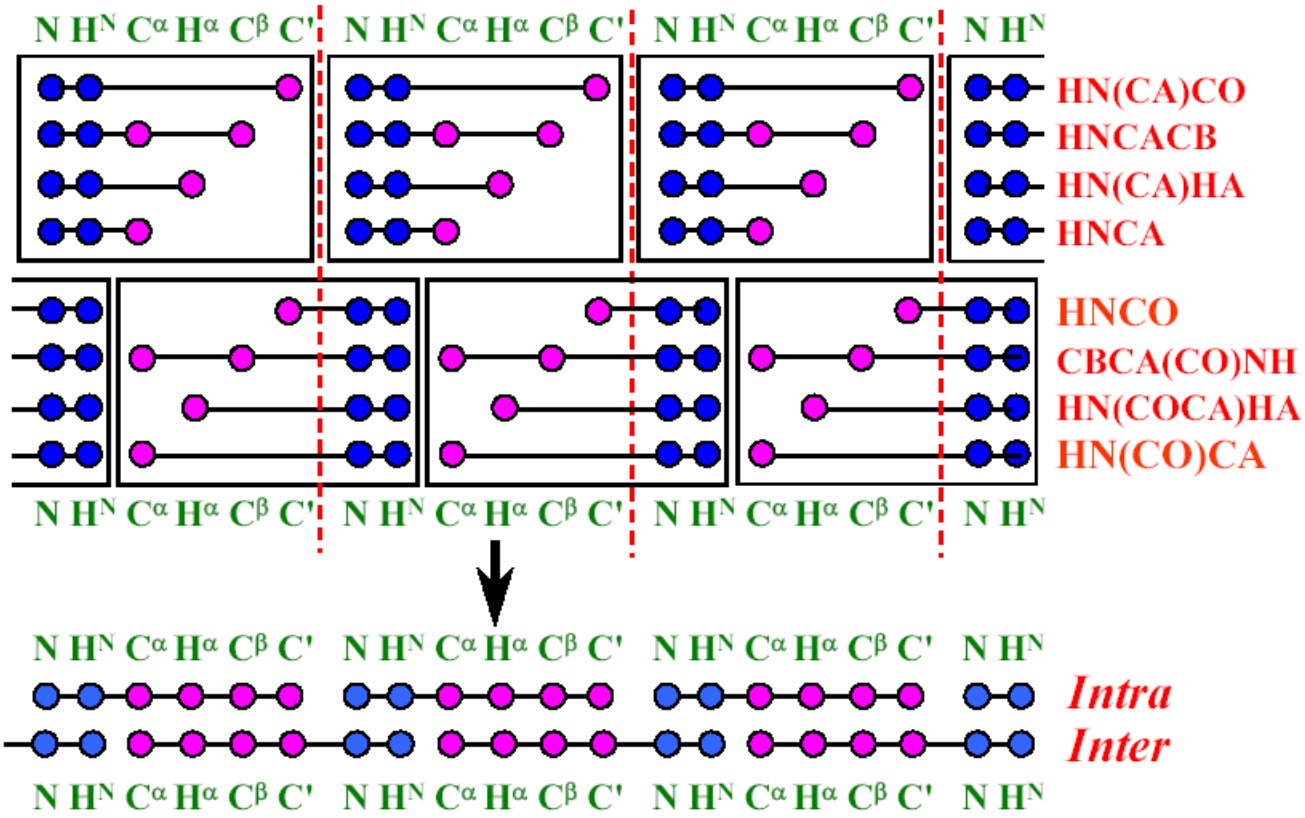
N H^N C^α H^α C^β C'
N H^N C^α H^α C^β C'
N H^N C^α H^α C^β C'
N H^N
HN(CA)CO
HNCACB
HN(CA)HA
HNCA
HNCO
CBCA(CO)NH
HN(COCA)HA
HN(CO)CA
N H^N C^α H^α C^β C'
N H^N C^α H^α C^β C'
N H^N C^α H^α C^β C'
N H^N
N H^N C^α H^α C^β C'
N H^N C^α H^α C^β C'
N H^N C^α H^α C^β C'
N H^N
Intra
Inter
N H^N C^α H^α C^β C'
N H^N C^α H^α C^β C'
N H^N C^α H^α C^β C'
N H^N

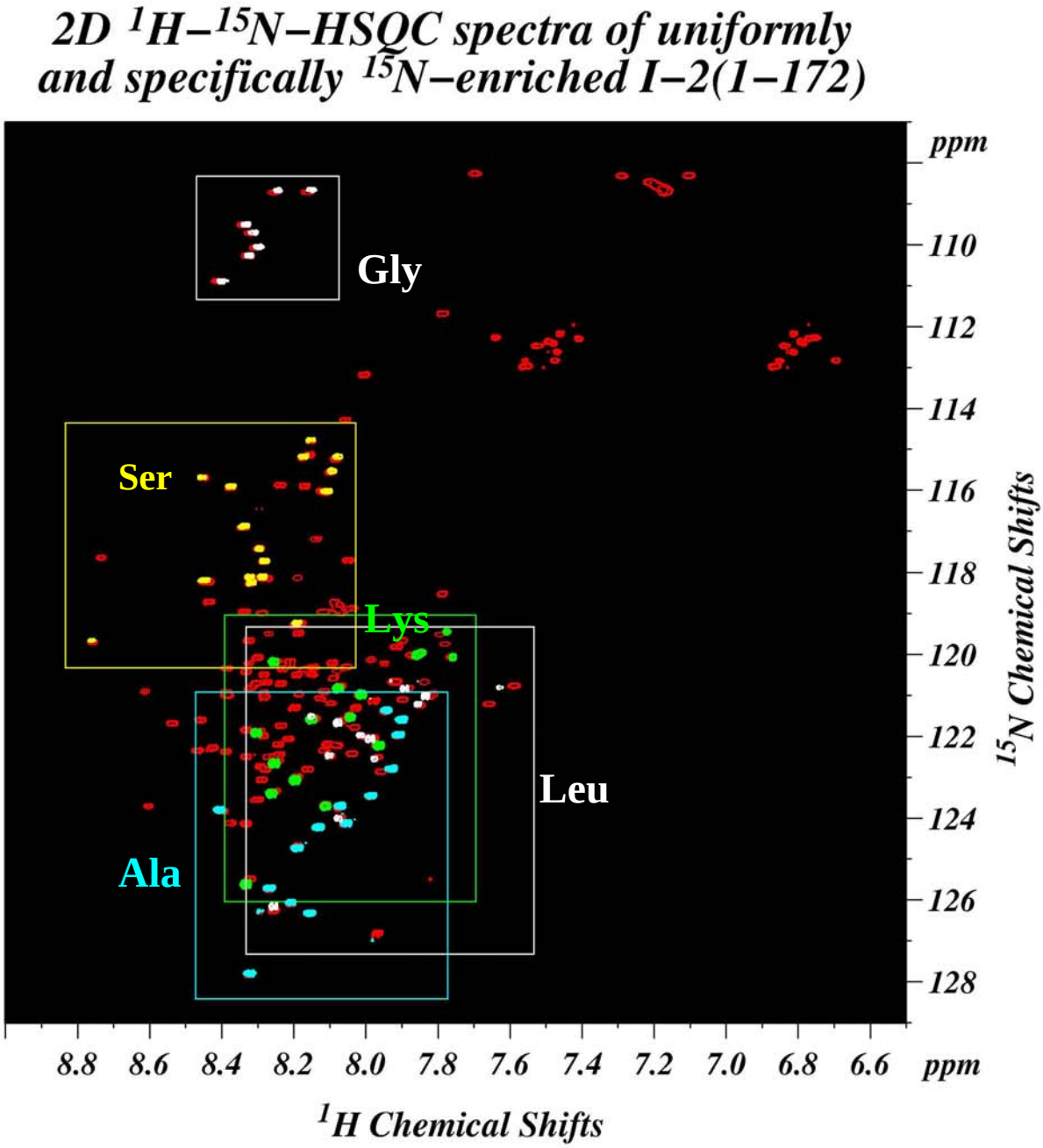
2D $^{1}H-^{15}N-HSQC$ spectra of uniformly and specifically $^{15}N-$enriched I–2(1–172)
Gly
Ser
Lys
Leu
Ala
ppm
110
112
114
116
118
120
122
124
126
128
^{15}N Chemical Shifts
8.8
8.6
8.4
8.2
8.0
7.8
7.6
7.4
7.2
7.0
6.8
6.6
ppm
^{1}H Chemical Shifts

Three-dimensional CBCA(CO)NH Spectrum

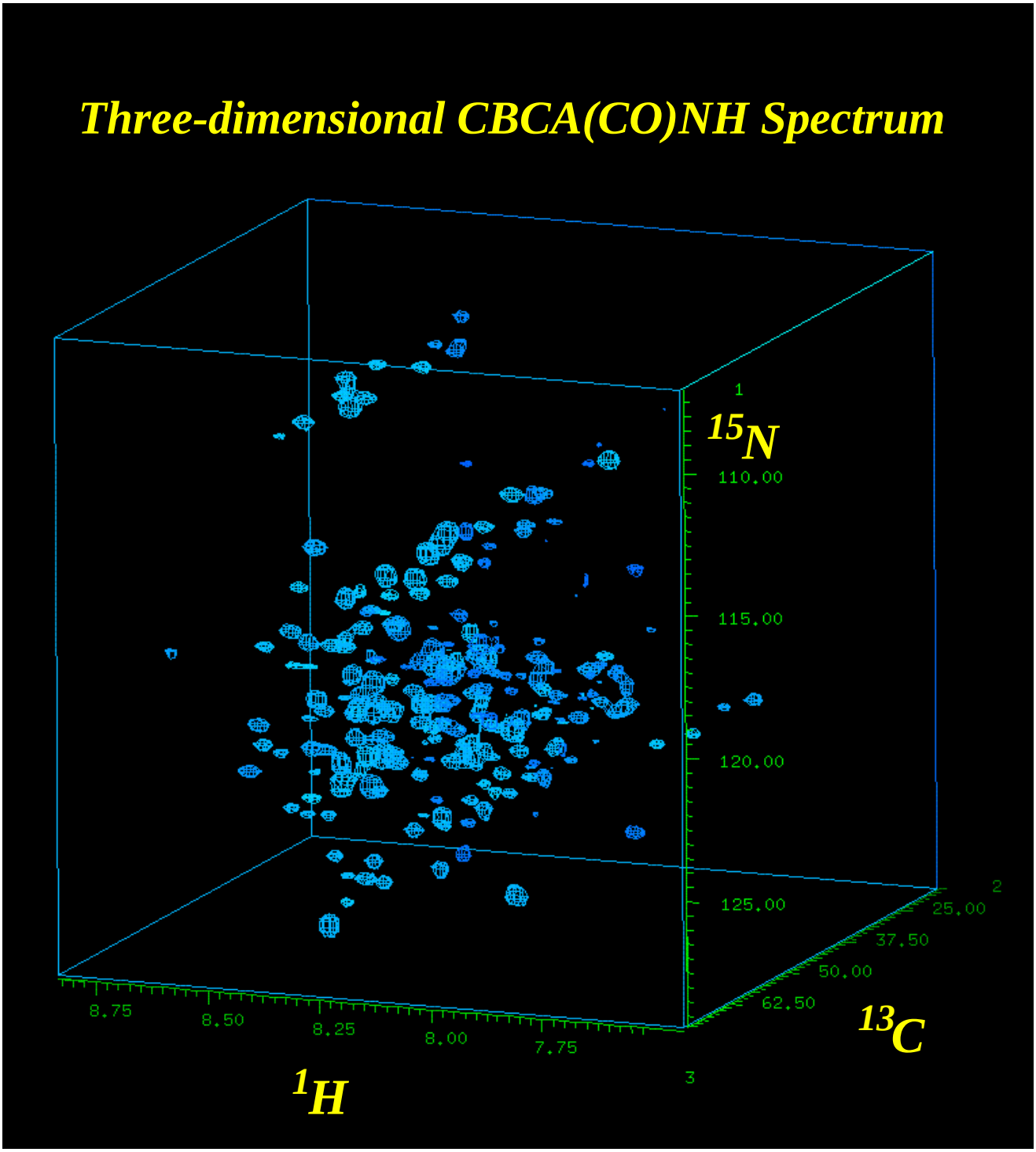

ω_2 (^{13}C), ω_3 (^{1}H) projection of three-dimensional CBCA(CO)NH spectrum

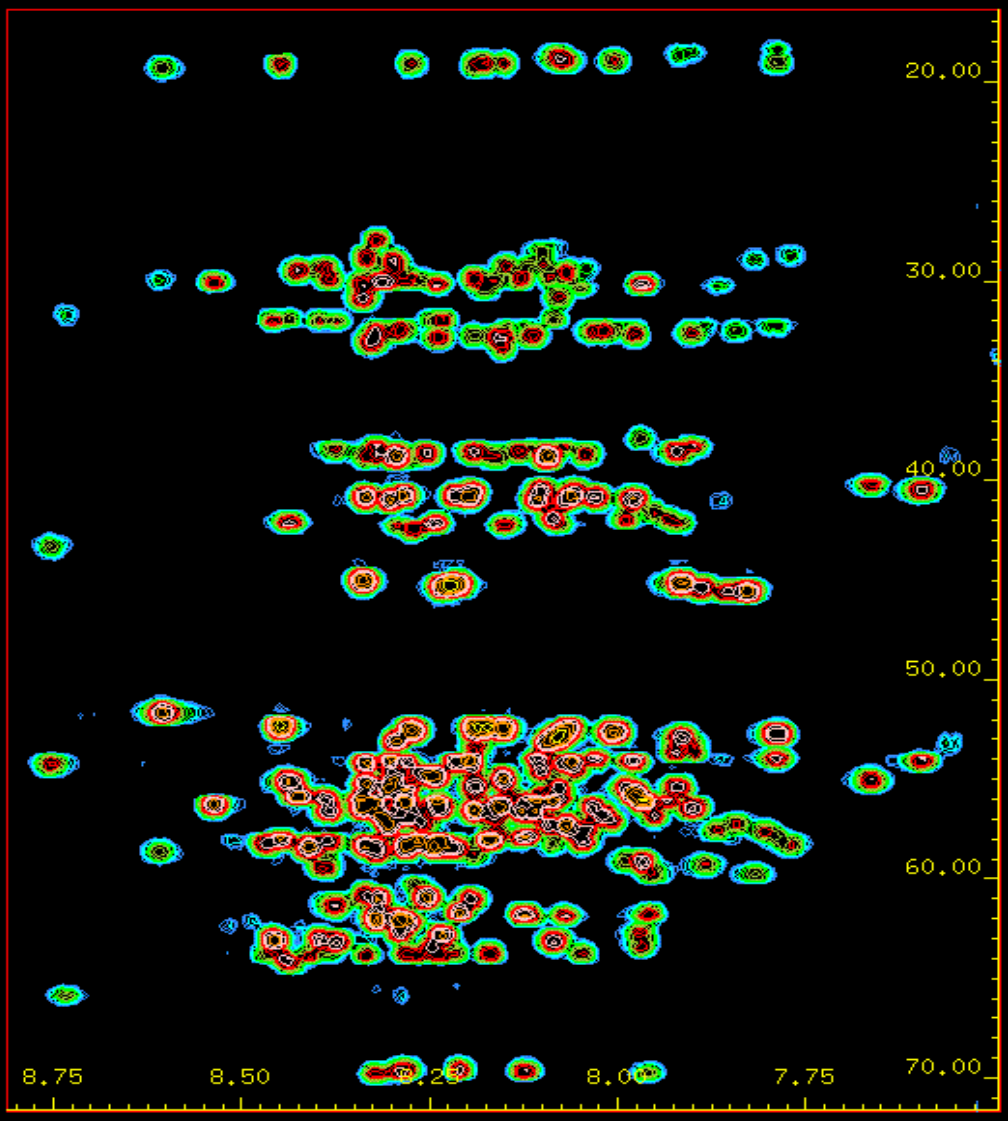

Strip plot of 3D CBCANH spectrum of inhibitor-2(1-172)

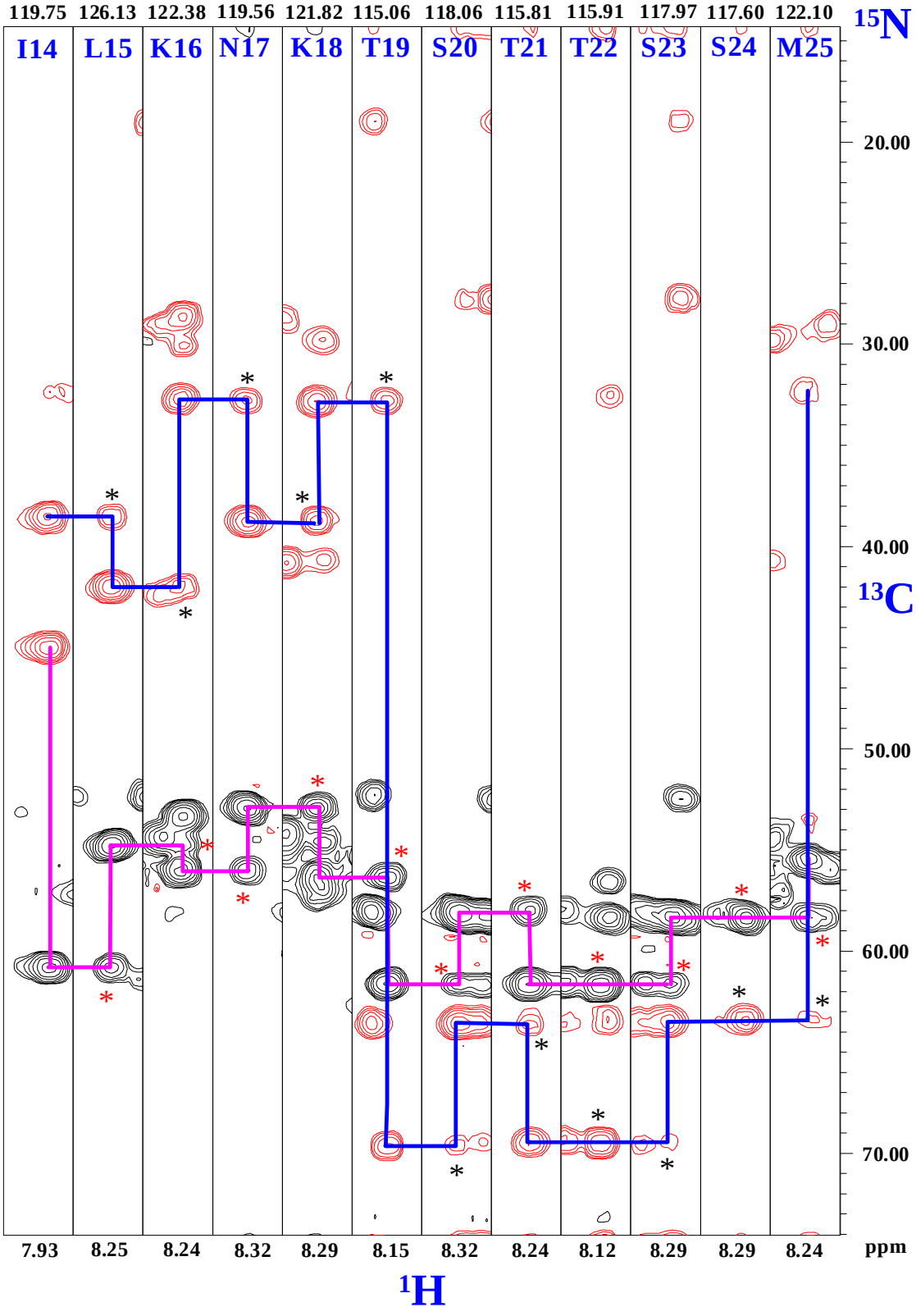

Strip plot of 3D HN(CA)CO spectrum of I-2(172)

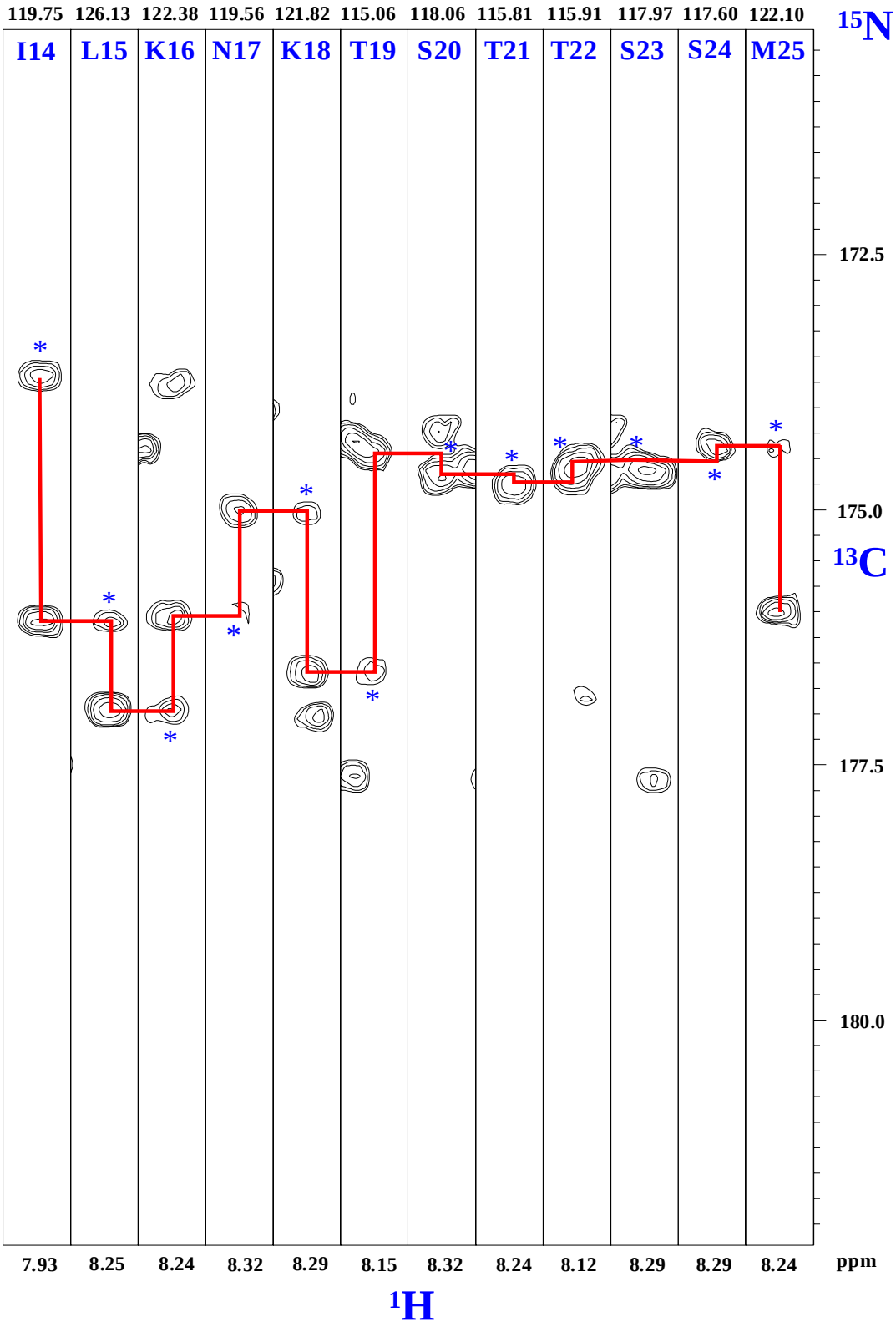

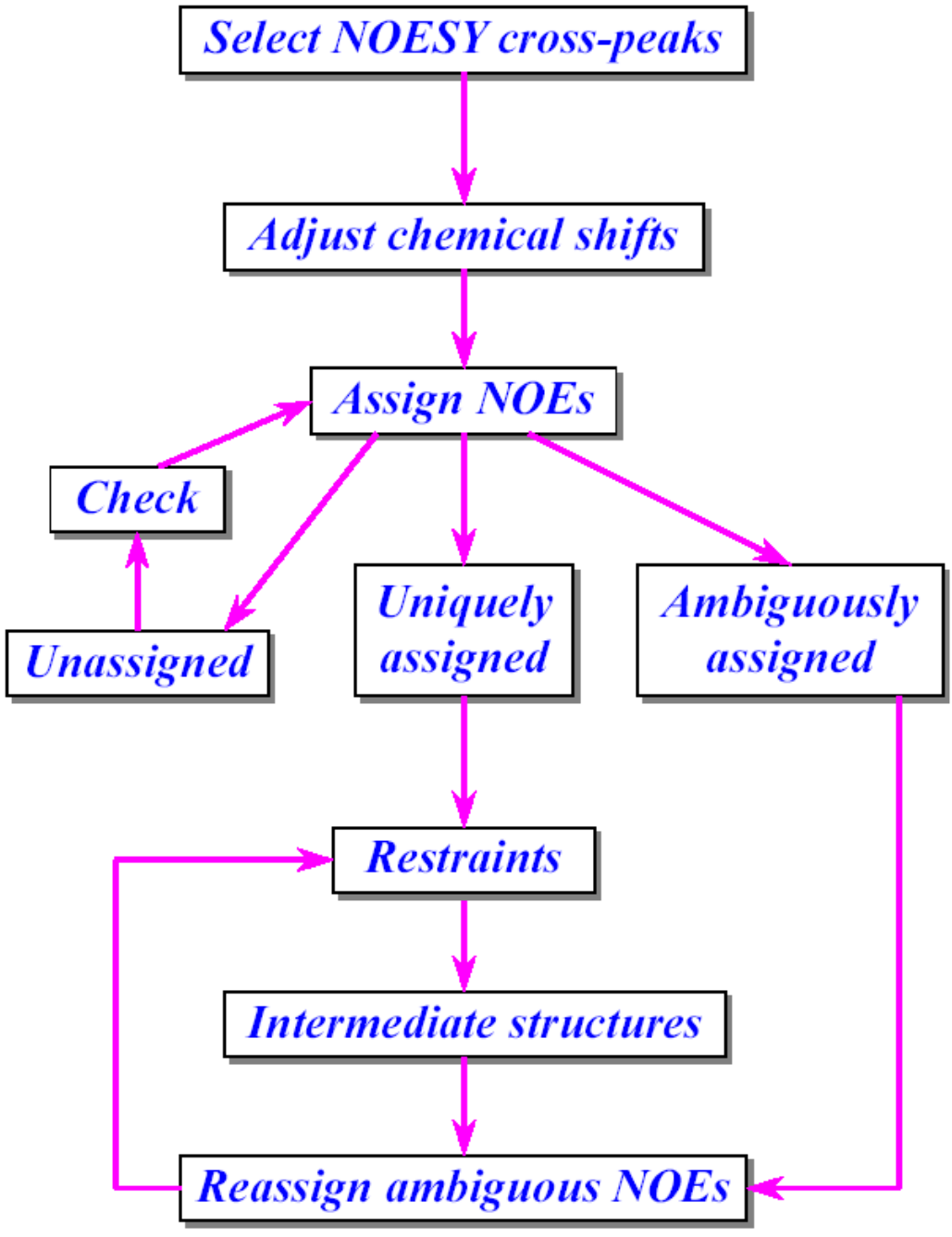
Select NOESY cross-peaks
Adjust chemical shifts
Assign NOEs
Check
Unassigned
Uniquely assigned
Ambiguously assigned
Restraints
Intermediate structures
Reassign ambiguous NOEs

Table 1. Structural statistics for the 20 final NMR structures of NRho

NMR constraints	
Distance constraints	
Total NOE	1830
Unambiguous	1469
Ambiguous	361
Intra-residue[a]	585
Inter-residue[a]	884
Sequential ($\|i–j\| = 1$)	344
Medium-range ($\|i–j\| \leq 4$)	305
Long-range ($\|i–j\| > 5$)	235
Hydrogen bonds[b]	54
Dihedral angles	
Φ	48
Ψ	48
Structure statistics[c]	
Violations	
NOE violations > 0.5 Å	0
Dihedral angle violations > 5°	0
Deviations from idealized geometry	
Bond lengths (Å)	$7.60 \times 10^{-3} \pm 2.38 \times 10^{-4}$
Bond angles (°)	0.96 ± 0.03
Impropers (°)	2.45 ± 0.09
Agreement with experimental restraints	
NOE	$5.46 \times 10^{-2} \pm 2.69 \times 10^{-3}$
Dihedral angles	0.81 ± 0.11
Average RMSD (Å)[d]	
Backbone[e]	0.45 ± 0.09 (0.25 ± 0.06)
Heavy atoms[e]	0.89 ± 0.08 (0.79 ± 0.13)
Ramachandran plot[f]	
Most favored (%)	69.8 (71.5)(92.9)
Additionally allowed (%)	22.0 (19.4)(7.1)
Generously allowed (%)	7.5 (9.1)(0.0)
Disallowed (%)	0.7 (0.0)(0.0)

[a] Splits shown only for unambiguous assignments.

[b] Hydrogen bond restraints were H^N–O distance of 1.8–2.3 Å and an N–O distance of 2.8–3.3 Å.

[c] Structural characteristics for the final ensemble of 20 water-refined structures.

[d] RMSD of the mean structure from individual structures in the ensemble.

[e] RMSD for residues 3–66 shown (these residues have $^1H^N$-{^{15}N}NOE at 800 MHz > 0.6). The numbers in the parentheses indicate the RMSD for regions with definite secondary structure.

[f] Ramachandran plot data shown for residues 3–66. The first set of numbers in parentheses indicates the statistics for the smaller subset after removal of residues (3, 5, 6, 7, 35, 36 and 42) shown to undergo a significant amount of conformational exchange. The second set indicates the characteristics for those residues in ordered regions of definite secondary structure.

Solid-state NMR application II

- macromolecules

(a) α-Spectrim SH3 domain

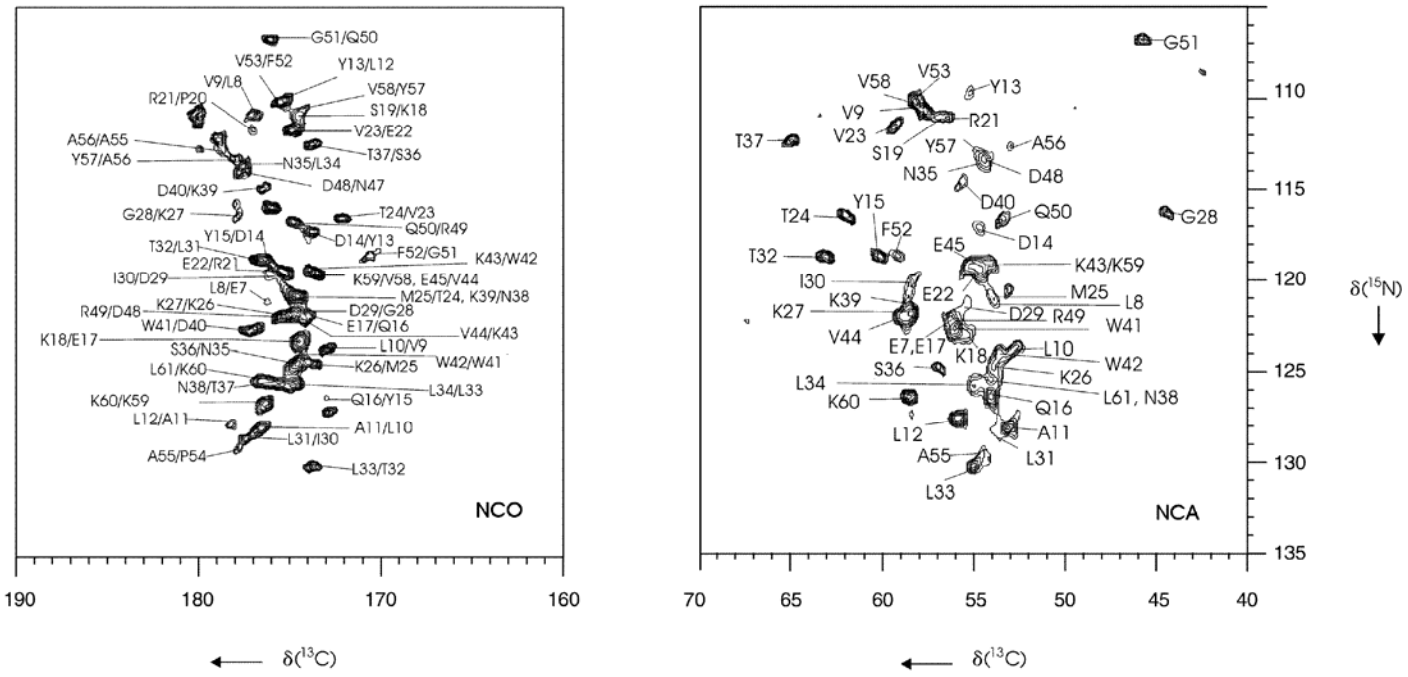

Figure 2. *NCO (left) and NCA (right) spectra of the precipitated α-spectrin SH3 sample recorded with the pulse sequence shown in Figure 1a with appropriate settings for carbon power and frequency. The spinning frequency was 12 kHz, and the temperature was adjusted to 278 K. Assigned signals are indicated with the respective residue type and number. In the spectrum at the left, the NCO cross peaks yielding sequential information are indicated with the residue contributing to the nitrogen chemical shift first, followed by the residue that contributes to the carbonyl chemical shift. Both spectra were processed to yield optimal resolution by applying a phase shifted by π/3 sine-bell function in* t_1 *and a Lorentz–Gauss transformation in* t_2.

Pauli et al., ChemBioChem., (2001), 2, 272-281

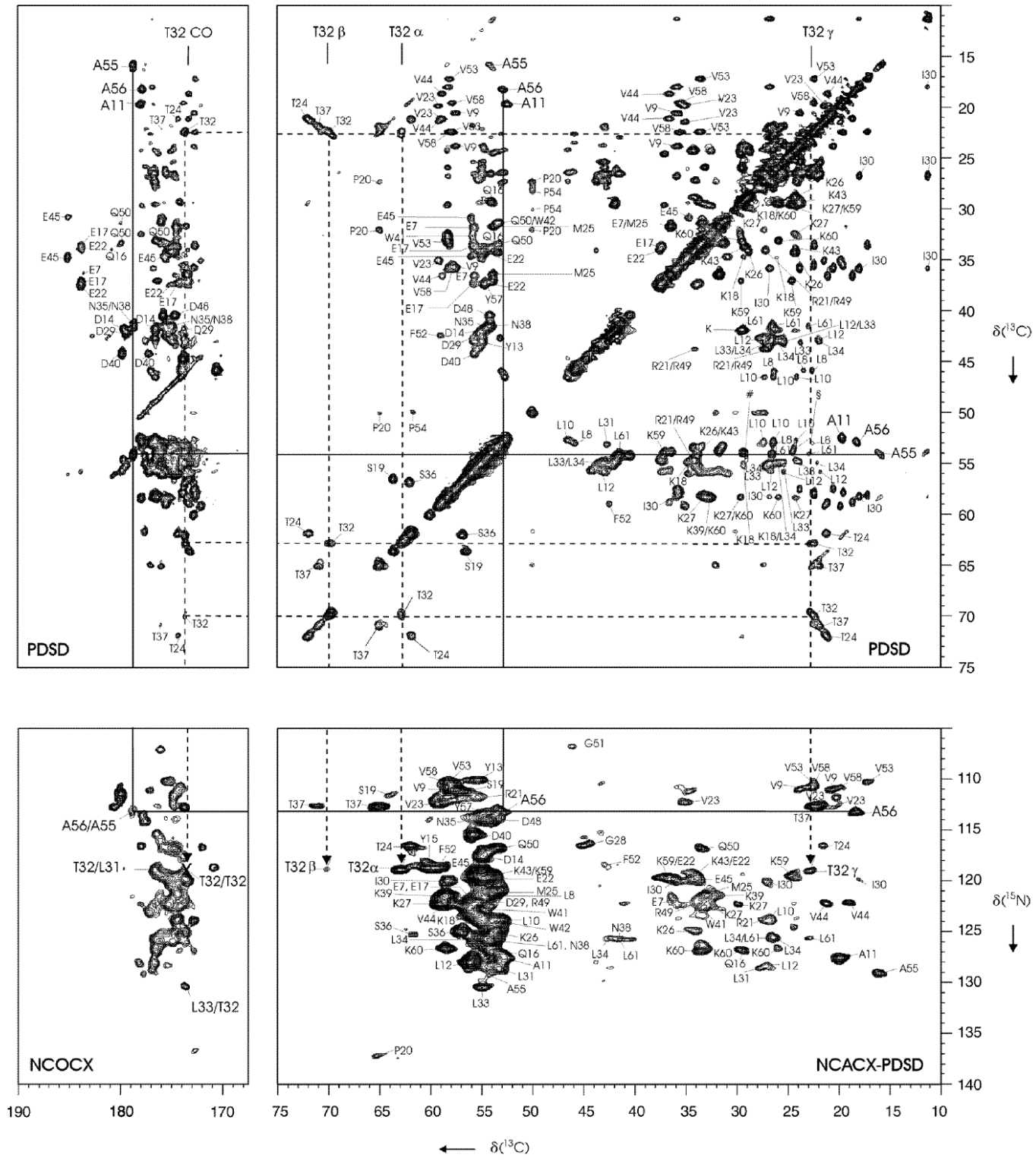

Pauli et al., ChemBioChem., (2001), 2, 272-281

Table 1. ^{13}C *and* ^{15}N *chemical shift values (δ) of the precipitated α-spectrin SH3 domain.*

Residue	^{15}N	^{13}CO	$^{13}C^{\alpha}$	$^{13}C^{\beta}$	$^{13}C^{\gamma}$	$^{13}C^{\delta}$	$^{13}C^{\varepsilon}$	$^{13}C^{\eta}$	$^{13}C^{\xi}$
E7	122.0	176.2	55.9	31.2	36.4				
L8	121.5	176.9	53.0	46.0	26.5	23.5/22.6			
V9	110.9	172.6	57.3	35.7	23.7/20.4				
L10	123.7	176.4	52.8	46.6	27.4	26.4/24.2			
A11	127.5	177.9	52.4	19.8					
L12	127.8	174.9	55.9	43.1	26.7	25.4/21.9			
Y13	110.0	173.8	55.2	43.5					
D14	117.4	176.5	54.6	41.8					
Y15	118.6	172.8	60.1	43.5					
Q16	126.5	174.0	53.8	29.6	33.8				
E17	122.0	174.4	55.7	33.4	37.3				
K18	123.4	174.6	55.0	34.8	26.2	29.4	42.0		
S19	111.3	173.3	56.5	63.7					
P20	137.2	177.0	65.0	32.1	27.3	50.1			
R21	112.0	175.2	55.2	34.1	27.2	43.9			
E22	119.3	174.8	54.8	33.9	37.5				
V23	112.2	172.0	59.1	35.0	21.3/19.8				
T24	116.4	174.3	61.8	71.8	21.3				
M25	121.1	173.5	53.8	36.4	31.7				
K26	125.0	174.9	53.7	34.2	24.4	28.8	42.0		
K27	122.2	177.9	58.5	32.5	24.3	29.7	42.0		
G28	116.3	173.9	44.6						
D29	121.8	175.0	55.1	42.2					
I30	119.8	176.7	58.3	35.9	26.8/18.1	11.4			
L31	128.4	177.0	53.3	42.5	28.1	27.4/26.4			
T32	118.8	173.8	62.7	69.8	22.5				
L33	130.1	174.4	55.0	43.0	26.8	25.5/23.8			
L34	125.7	177.6	55.0	43.0	26.8	26.0/22.2			
N35	113.9	174.6	54.4	41.5					
S36	124.8	173.5	56.8	62.0					
T37	112.6	175.7	65.0	70.9	21.6				
N38	126.0	174.8	54.0	41.6					
K39	121.4	176.2	58.2	33.4					
D40	115.3	177.2	55.7	44.4					
W41	122.7	174.2	55.9	32.9	111.0	128.5/128.5	139.0/118.7	114.8/121.0	125.7
W42	123.6	174.8	53.5	31.6	112.2	126.1/129.3	139.3/121.1	114.7/119.9	124.3
K43	119.6	174.8	54.0	33.8	24.2	29.3	42.0		
V44	121.9	173.1	59.3	36.4	21.0/18.6				
E45	120.0	175.5	56.1	30.9	34.8				
V46			59.9	33.1	20.8/19.8				
N47		177.5	55.0						
D48	113.9	174.6	54.1	40.5					
R49	122.2	176.6	55.2	34.1	27.2	43.9			
Q50	116.6	175.9	53.1	31.6	33.3				
G51	106.8	170.5	45.9						
F52	118.6	175.3	58.8	42.5	140.2	131.5/131.5	131.4/131.4		129.3
V53	110.0	172.6	57.9	33.5	22.3/17.0				
P54	136.8	177.7	61.6	30.1	28.3	50.0			
A55	129.0	178.7	54.0	15.9					
A56	113.0	177.7	52.8	18.2					
Y57	113.4	174.4	54.8	37.2	133.3	118.5	130.8		159.5
V58	110.7	173.8	57.8	35.5	22.4/19.8				
K59	119.6	176.4	54.0	37.2	24.7	29.6	42.0		
K60	126.7	176.6	58.4	33.4	26.0	29.6	42.0		
L61	125.7	175.6	54.3	41.4	29.4	26.6/23.0			
D62									

Pauli et al., ChemBioChem., (2001), 2, 272-281

α-^{13}C Chemical Shift Values Categorized According to Secondary Structural Assignment[a-d]

Residue[e] type	Helix (DDS)	β Strand (DDS)	Coil (DDS)	Spera (1991) (TSP)	Richarz (1978) (dioxane)
Ala (112)	54.7	50.3	52.4	52.3	50.8
Cys (27)	60.0	56.1	56.0	56.9	53.9
Asp (97)	56.7	52.3	54.2	54.0	52.7
Glu (132)	59.2	54.6	56.4	56.4	55.4
Phe (74)	60.7	56.1	57.8	58.0	56.2
Gly (121)	46.5	44.6	45.4	45.1	43.9
His (24)	58.5	55.1	55.5	-	53.6
Ile (86)	64.7	59.8	61.3	61.3	59.6
Lys (138)	59.3	54.8	56.6	56.5	54.6
Leu (113)	57.8	53.9	55.7	55.1	53.8
Met (36)	57.8	54.1	55.7	55.3	54.0
Asn (71)	55.8	51.9	55.7	52.8	51.5
Pro (53)	65.9	62.5	53.2	63.1	61.9
Gln (61)	58.7	54.0	55.8	56.1	54.1
Arg (65)	59.4	54.8	56.7	56.1	54.6
Ser (88)	61.2	56.8	58.2	58.2	56.6
Thr (105)	65.8	60.6	62.0	62.1	60.1
Val (114)	65.7	60.0	62.3	62.3	60.7
Trp (12)	59.0	55.2	56.4	57.7	55.7
Tyr (43)	60.7	56.6	57.5	58.1	56.3

[a] Experimentally measured random coil values from Richarz and Wuthrich and from Spear and Bax are included for comparison. Data are given in ppm.

[b] The compounds (DDS, TMS, or dioxane) used in referencing the data are shown at the top of each column.

[c] To adjust DSS values to “old” dioxane standard, substract 1.5 ppm.

[d] To adjust DSS values to TSP, add 0.1 ppm.

[e] Total number of residues observed is given in parentheses. The data cover a grand total of 1572 amino acids.

Random Coil Chemical Shifts for Backbone Atoms in Peptides and Proteins[a]

Residue	α-^{1}H[b]	N-^{1}H	2-^{13}C	1-^{13}C	^{15}N
Ala	4.33	8.15	52.2	177.6	122.5
Cys	4.54	8.23	56.8	174.6	118.0
Asp	4.71	8.37	53.9	176.8	120.6
Glu	4.33	8.36	56.3	176.6	121.3
Phe	4.63	8.30	57.9	175.9	120.9
Gly	3.96	8.29	45.0	173.6	108.9
His	4.60	8.28	55.5	174.9	119.1
Ile	4.17	8.21	61.2	176.5	123.2
Lys	4.33	8.25	56.4	176.5	121.5
Leu	4.32	8.23	55.0	176.9	121.8
Met	4.48	8.29	55.2	176.3	120.5
Asn	4.74	8.38	52.7	175.6	119.5
Pro	4.42	-	63.0	176.0	128.1
Gln	4.33	8.27	56.0	175.6	120.3
Arg	4.35	8.27	56.0	176.6	120.8
Ser	4.47	8.31	58.1	174.4	116.7
Thr	4.35	8.24	62.0	174.8	114.2
Val	4.12	8.19	62.2	176.0	121.1
Trp	4.66	8.18	57.6	173.6	120.5
Tyr	4.55	8.28	58.0	175.9	122.0

[a] Proton and carbon shifts are relative to DDS, nitrogen shifts are relative to NH_3. Data are given in ppm.

[b] α-^{1}H shifts were measured using the hexapeptide GGXAGG in 1M urea at 25C.

Wishart and Skyes, Methods Enzymol. (1994), **239** ,363-392.

Dipolar splitting and Chemical shifts

$$\begin{aligned}\mathbf{F}(\rho, \tau) &= (\text{chemical shift}(\rho, \tau), \text{dipolar splitting}(\rho, \tau)) \\ &= (\sigma_{11}(-0.828 \cos\rho \sin\tau + 0.558 \sin\rho \sin\tau \\ &\quad - 0.047 \cos\tau)^2 + \sigma_{22}(0.554 \cos\rho \sin\tau \\ &\quad + 0.803 \sin\rho \sin\tau - 0.220 \cos\tau)^2 \\ &\quad + \sigma_{33}(-0.088 \cos\rho \sin\tau - 0.206 \sin\rho \sin\tau \\ &\quad - 0.975 \cos\tau)^2, \frac{\nu_{\|}}{2}(3(-0.326 \cos\rho \sin\tau \\ &\quad - 0.034 \sin\rho \sin\tau - 0.946 \cos\tau)^2 - 1))\end{aligned} \quad [1]$$

For a tilted helix, the plot of the PISA wheels is generated by graphing the set

$$S(\tau) = \{\mathbf{F}(\rho, \tau): \rho \in [0, 2\pi)\}. \quad [2]$$

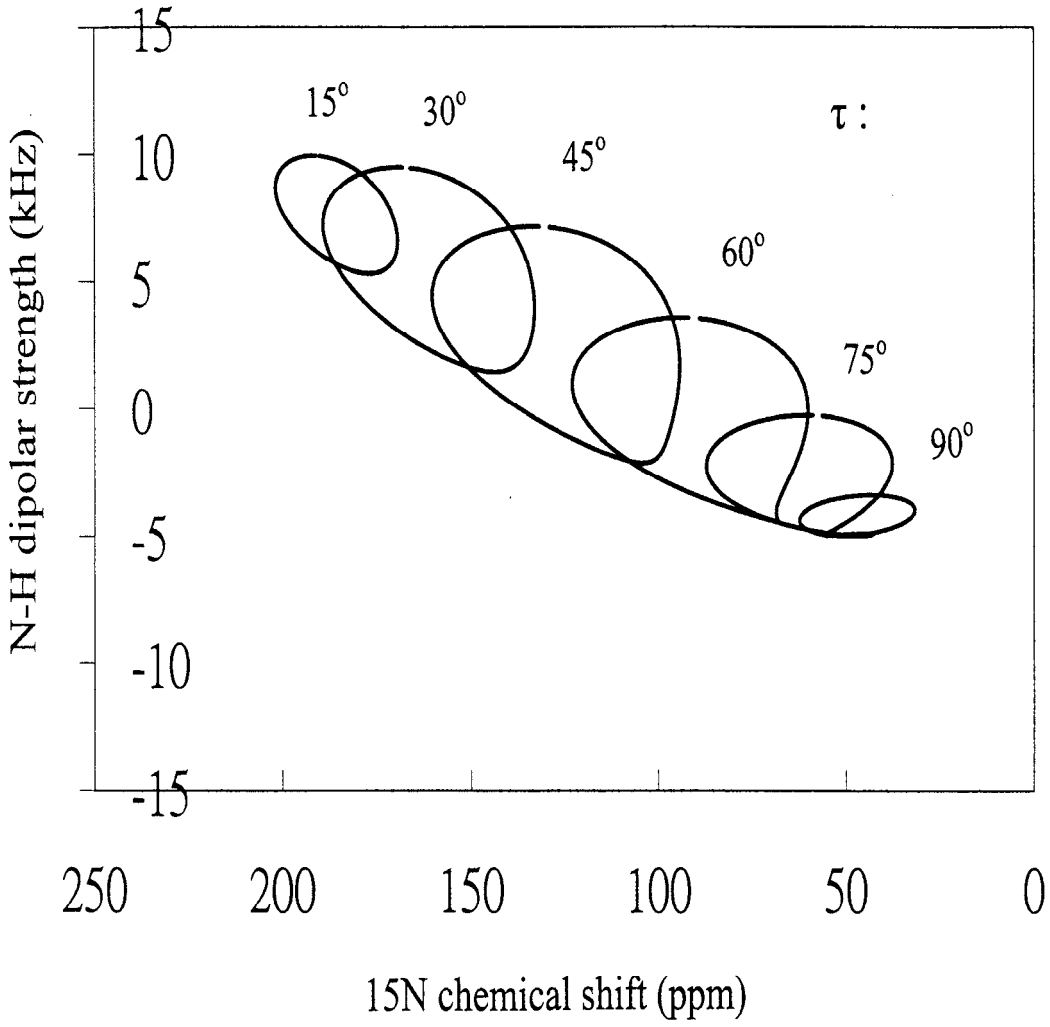

Fig. 4. "Circles" represents the wheel pattern corresponding to each tilted helix structure, where the slant angle was specific in figure. Average tensor elements (σ_{11}=31.3, σ_{22}=55.2, σ_{33}=201.8) in ppm, dipolar strength of 25 kHz and the relative orientation of the dipolar and chemical shift tensor of 17° were used in simulation.

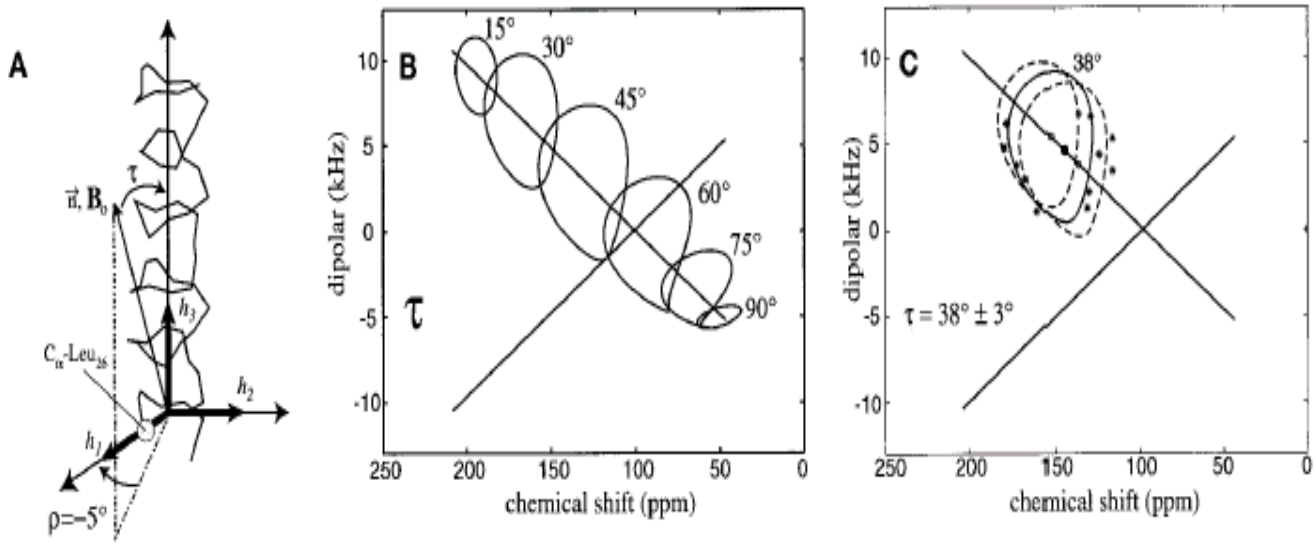

FIG. 2. The origins of the "PISA wheels." For the analysis in this manuscript, n, the bilayer normal, is always aligned parallel to B_0. (A) Definitions of τ and ρ for an α-helix. $\tau = 0°$ occurs when the helix axis, h_3, is parallel to B_0. $\rho = 0°$ occurs when the projection of B_0 onto a plane perpendicular to h_3 makes an angle of 0° with h_1, the radial axis of the helix that passes through the C_α carbon of Leu_{26}. (B) "Circles" drawn for one of the dipolar transitions using average values of tensor elements ($\tau_{11} = 31.3$, $\tau_{22} = 55.2$, $\sigma_{33} = 201.8$ ppm) and the relative orientations of the dipolar and chemical shift tensor, given by $\theta = 17°$, the angle in the peptide plane between σ_{33} and $\nu_{\parallel}$ (parallel to the N–H bond). The circles for the other dipolar transitions are the mirror image about 0 kHz. (C) Characterization of the M2-TMP helix tilt from a more complete set of PISEMA data than that presented in Fig. 1. The data are consistent with a helix tilt of 38 ± 3°. Note that the center of the PISA wheels falls on a line that passes through the isotropic chemical shift (96 ppm) at 0 kHz on the dipolar scale.

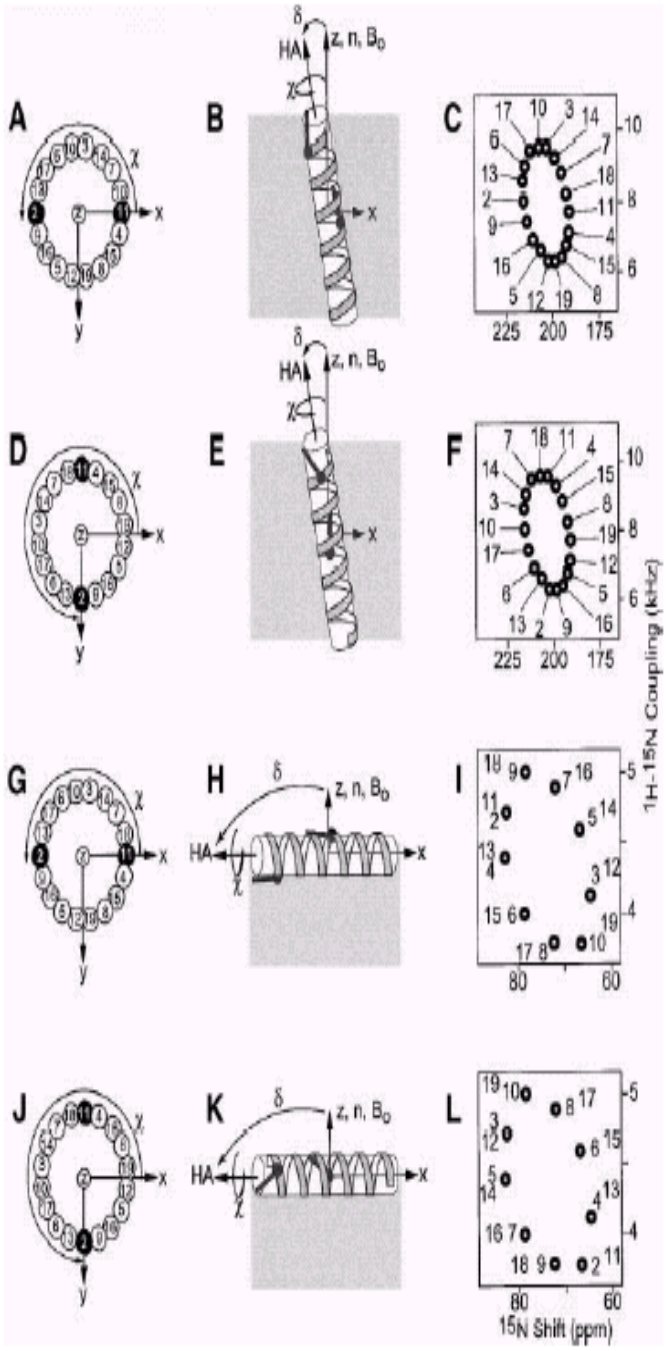

FIG. 3. Correspondence between membrane protein helix tilt and polarity, and the resulting PISEMA spectra for uniformly ^{15}N-labeled protein in oriented bilayers. A, D, G, and J. Helical wheels rotated by various values of the polar angle χ. B, E, H, and K. Helices rotated through various values of χ about their long axes (HA) and tilted by $\delta = 12°$ (B, E) and $\delta = 90°$ (H, K) away from the membrane normal (n). The *y* axis of the laboratory frame points out of the page. C, F, I, and L. Calculated PISEMA spectra for the various helix rotations and tilts. The NH bond vectors of the polar opposite residues 2 and 11 in the helical wheels are highlighted. The light gray areas in B, E, H, and K represent the lipid bilayer.

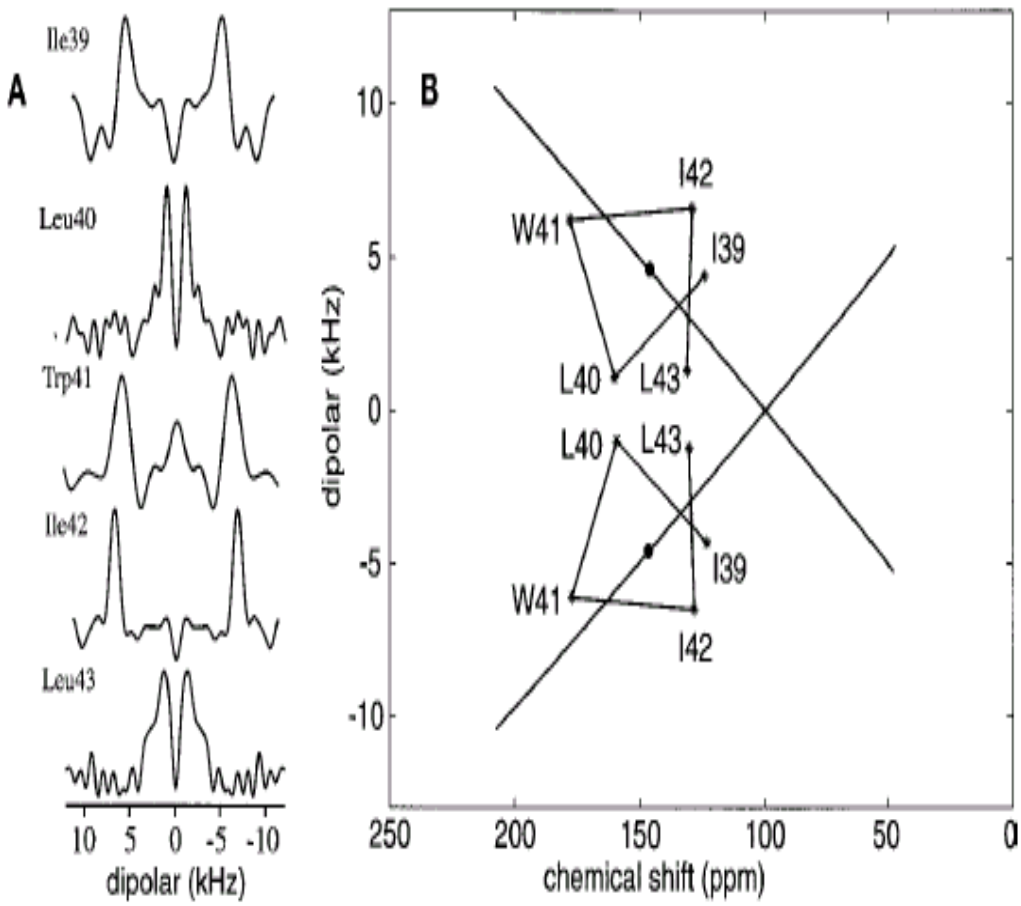

FIG. 1. (A) Dipolar splittings observed from PISEMA spectra of multiple and single site labeled preparations of M2-TMP in hydrated lipid bilayers aligned with the bilayer normal parallel to the magnetic field direction. The spectra were obtained (Song *et al.*, unpublished results) with a 400-MHz spectrometer using a Chemagnetics data acquisition system and a 9.4-T wide-bore Oxford Instruments magnet. An RF field strength of 38.5 kHz was used for the Lee–Goldburg (LG) condition corresponding to a LG time increment of 26 μs. A delay of 1 μs was given at the onset of each $\pm$LG cycle to compensate for the frequency synthesizer (PTS) switch time. The t_1 duration was incremented from 0 to 24 LG cycles and the refocused ^{15}N signal was typically acquired with 2000 transients for each t_1 increment. Spectral symmetry in the dipolar dimension was achieved by setting the imaginary part of the data to zero before the Fourier transform against t_1. The experimental error in the chemical shift dimension is $\pm$5 ppm and in the dipolar dimension it is $\pm$1 kHz. (B) Display of the dipolar splittings (*) at their observed chemical shift. The resonances are connected in helical wheel fashion. Since the two wheels are mirror images displaying identical information, only one will be used in the following figures.

Determination of rotational orientation of the helix, ρ

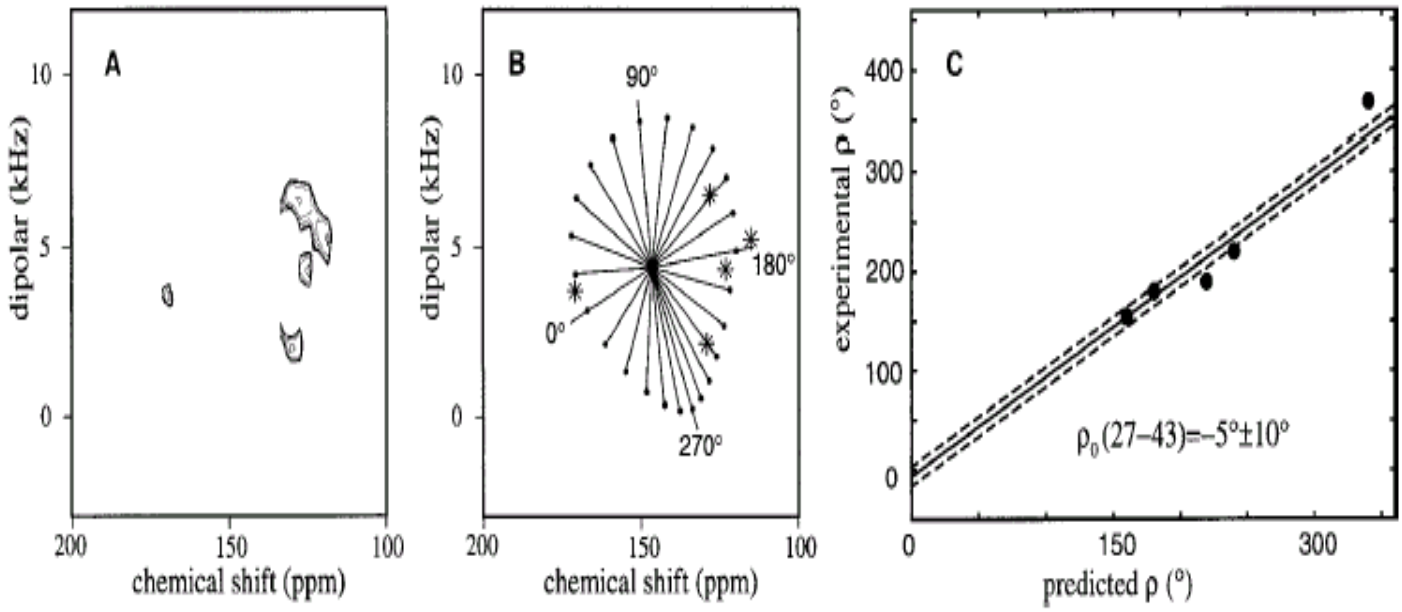

FIG. 3. (A) The ^{15}N Ile$_{32,33,35,39,42}$-labeled M2-TMP PISEMA spectrum obtained as in Fig. 1. Most of the resonances have been assigned based on single-site isotopic labels, but here the analysis has no dependence on such assignments. (B) Based on Eq. [1], the "PISA wheels" can be dissected into domains of ρ angles for cataloging an experimental value of ρ for each resonance. (C) The experimental ρ values are compared to predicted values based on residue number and 100°/residue for an ideal helix. Predicted and experimental values are paired by solving for a best fit. The result is an extrapolation and intersection with the experimental axis at $\rho_0 = -5 \pm 10°$.

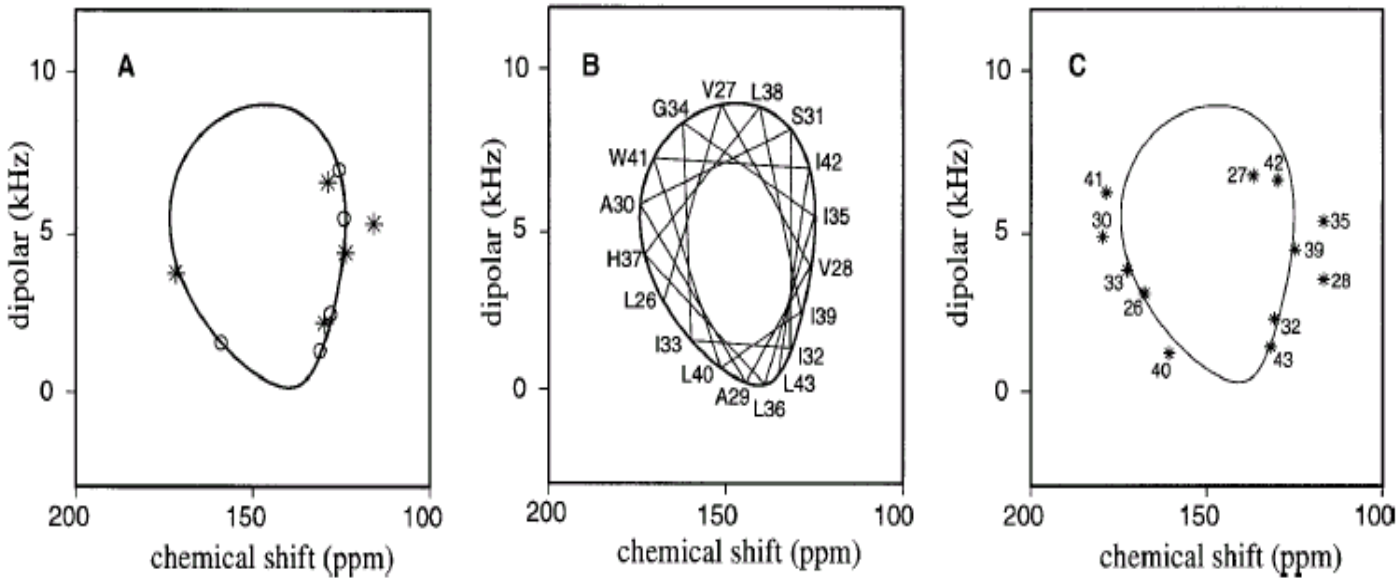

FIG. 4. (A) Best fit (○) to the 5-site Ile-labeled M2-TMP PISEMA resonances (*) based on the analysis in Fig. 3. (B) From this analysis and the resulting assignment of resonances, the helical wheel for this hydrophobic transmembrane peptide can be predicted. (C) The predicted resonance positions from the helical wheel are compared to the experimental data.

TABLE 1
Chemical Shift Tensor Element Magnitudes for the Observed Sites in M2-TMP[a]

Site	σ_{11}	σ_{22}	σ_{33}
Val27	33	55	198
Val28	29	53	202
Ile32	35	59	208
Ile33	31	54	202
Ile35	32	56	210
Ile39	30	54	195
Leu40	32	55	203
Trp41	32	56	205
Ile42	30	54	198
Leu43	29	56	200

[a] The chemical shift anisotropy has been determined from single site labeled samples of M2-TMP. Spectra were obtained of samples dried from trifluoroethanol where the peptide is observed to be α-helical; it is likely, therefore, that the peptides for this characterization are in the conformation of interest.

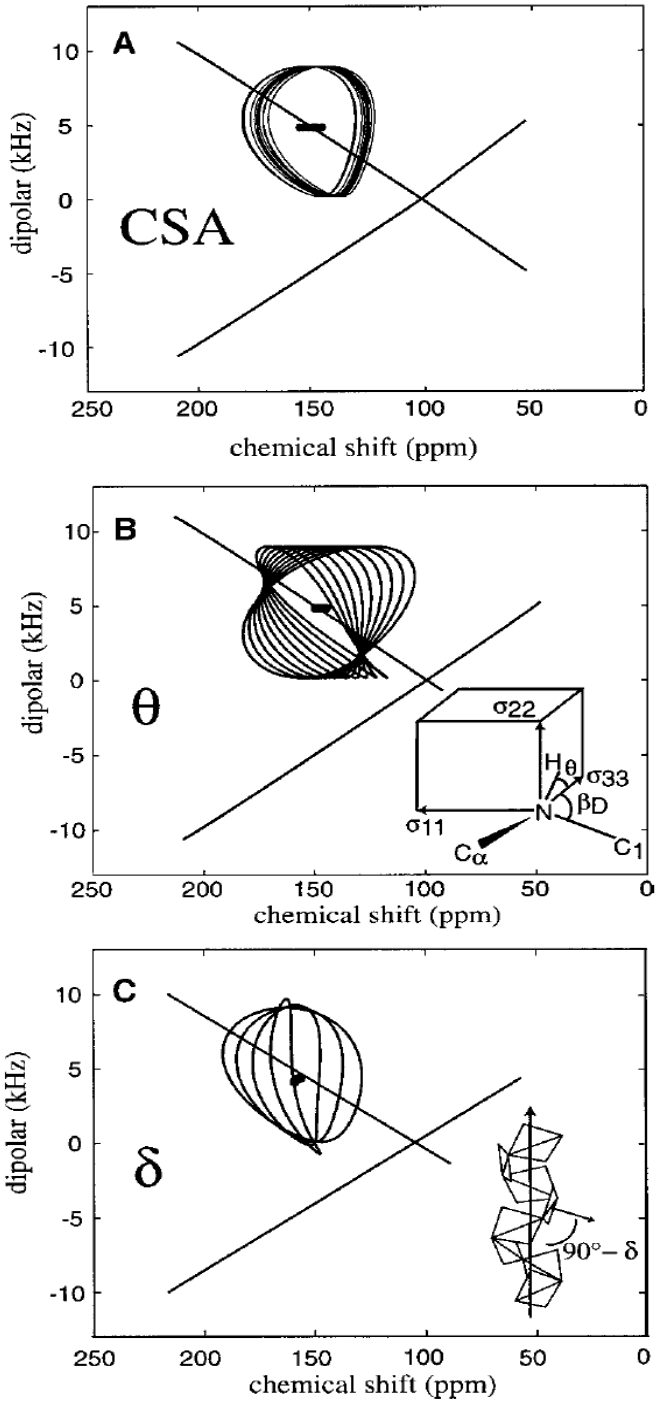

FIG. 5. The chemical shift anisotropy (CSA), relative orientation of chemical shift and dipolar tensors (θ), and local variation in helical structure through compensated peptide plane tilts (δ) are potential sources of distortion for the PISA wheel. (A) The chemical shift anisotropy has been determined from single site labeled samples of M2-TMP. The calculation of a "PISA wheel" using each of these CSA tensors (Table 1) is displayed showing significant variation in both the pattern and the calculation of its center. (B) The influence of θ on the PISA wheel is dramatic, but shows little effect on the pattern's center. The range of θ values displayed is 5 to 23° in 2° increments, where $\theta + \beta_D = 122°$, the HNC_1 bond angle. The value $\theta = 17°$ corresponding to $\beta_D = 105°$ has been used in all other figures. (C) The influence of peptide plane tilt on the shape of the PISA wheel is also dramatic, but there is little effect on the center of the pattern. The δ values displayed are 0, 5, 8.7, and 12°. The ideal helix has peptide plane tilts of $\delta = 8.7°$, the value used in all other figures.

Multiple quantum solid-state NMR indicates a parallel, not antiparallel, organization of β-sheets in Alzheimer's β-amyloid fibrils

Oleg N. Antzutkin*†, John J. Balbach*, Richard D. Leapman‡, Nancy W. Rizzo‡, Jennifer Reed*, and Robert Tycko*§

*Laboratory of Chemical Physics, National Institute of Diabetes and Digestive and Kidney Diseases, National Institutes of Health, Bethesda, MD 20892-0520; †Division of Inorganic Chemistry, Luleå University of Technology, Luleå, Sweden S-971 87; and ‡Division of Bioengineering and Physical Science, Office of Research Services, National Institutes of Health, Bethesda, MD 20892

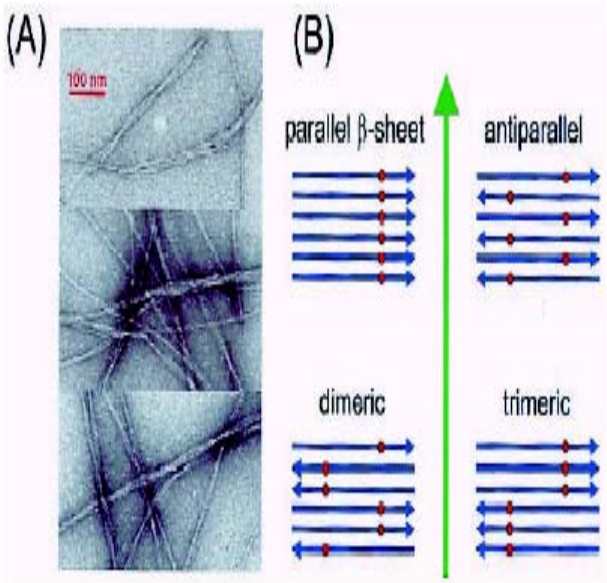

Fig. 1. (*A*) Electron micrographs of negative-stained $A\beta_{1-40}$ fibrils adsorbed to carbon films from an $A\beta_{1-40}$ solution after incubation at 24°C and pH 7.4 for 3 days. Typical amyloid fibrils are observed, appearing as single filaments or bundles of filaments with overall diameters ranging from 8 to 20 nm and with twist periodicities between 40 and 150 nm. The same solution, in which the $A\beta_{1-40}$ peptides were labeled with ^{13}C at the methyl carbon of Ala-21, subsequently was lyophilized for MQNMR measurements shown in Fig. 2. (*B*) $A\beta_{1-40}$ fibrils are believed to have a predominantly β-sheet structure with peptide chains (blue arrows) approximately perpendicular to and hydrogen bonds approximately parallel to the long axis of the fibril (green arrow). Four candidates for the supramolecular organization of the fibrils are shown. These can be distinguished experimentally by incorporating ^{13}C labels (red dots) at a single site in the peptide and measuring ^{13}C multiple quantum NMR spectra, because observation of an *n*-quantum signal requires that at least *n* ^{13}C nuclei be close enough in space to have significant magnetic dipole-dipole couplings.

Materials and Methods

Sample Preparation. Peptides with the human $A\beta_{1-40}$ sequence DAEFRHDSGYEVHHQKLVFFAEDVGSNKGAIIGLMVGGVV were synthesized, purified, and fibrillized from 0.25- to 1.0-mM solutions at pH 7.4 as described (11, 12). Fibrillized solutions were lyophilized for solid state NMR measurements. Typical solid state NMR samples were 10 mg. For EM, fibrillized solutions were diluted by a factor of 10–20 and negatively stained with uranyl acetate as described (11, 13).

The following samples were synthesized with uniform ^{15}N and ^{13}C labeling of the specified residues: SU7 (F19, V24, G25, A30, I31, L34, M35), SU6 (A2, D7, G9, Y10, V12, M35), SU5 (D23, K28, G29, I32, V36), and CU6 (K16, L17, V18, F19, F20, A21). The following samples were synthesized with ^{13}C labels at the specified pairs of backbone carbonyl sites: DL1 (D23, V24), DL2 (V24, G25), DL3 (G25, S26), DL4 (K28, G29), and DL5 (G29, A30). The notations SUn, CUn, and DLn indicate "scattered uniform" labeling of *n* residues, "consecutive uniform" labeling of *n* residues, and the *n*th "double labeled" sample, respectively.

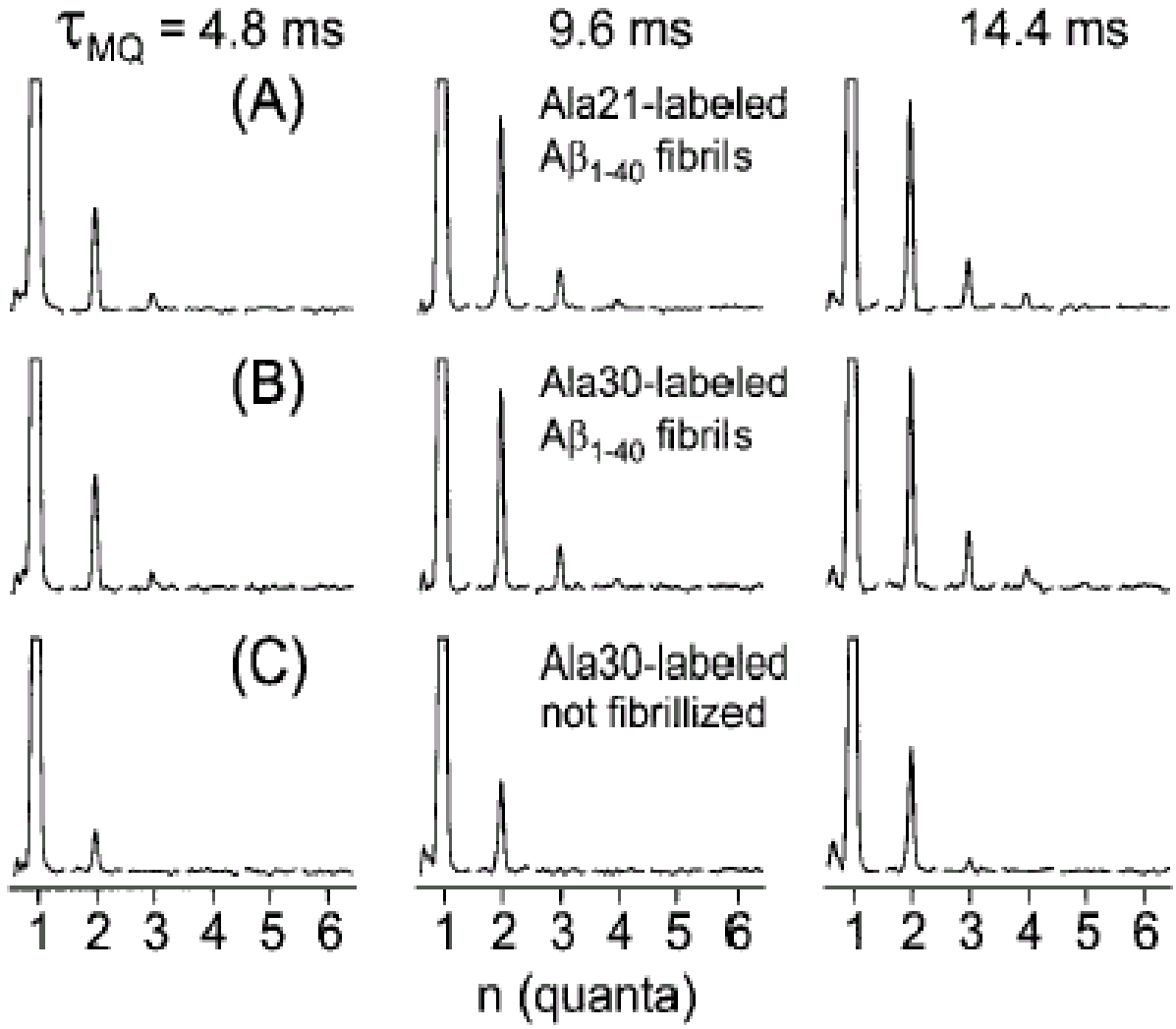

Fig. 2. ^{13}C MQNMR spectra of fibrillized and unfibrillized $A\beta_{1-40}$ samples, shown in order of increasing MQ excitation time τ_{MQ}. Each MQ spectrum is displayed as a series of subspectra for MQ orders from 1 to 6, with a spectral window from −15 kHz to + 15 kHz in each subspectrum. Vertical scales are adjusted so that one-quantum peaks are clipped at 25% of their maximum values. In the fibrillized samples (*A* and *B*), the amplitudes of two-, three-, and four-quantum signals increase with increasing τ_{MQ}. Spectra of samples with ^{13}C labels at methyl carbons of Ala-21 and Ala-30 are nearly identical. In unfibrillized samples (*C*), the three-quantum amplitude is small and no four-quantum signal is observed.

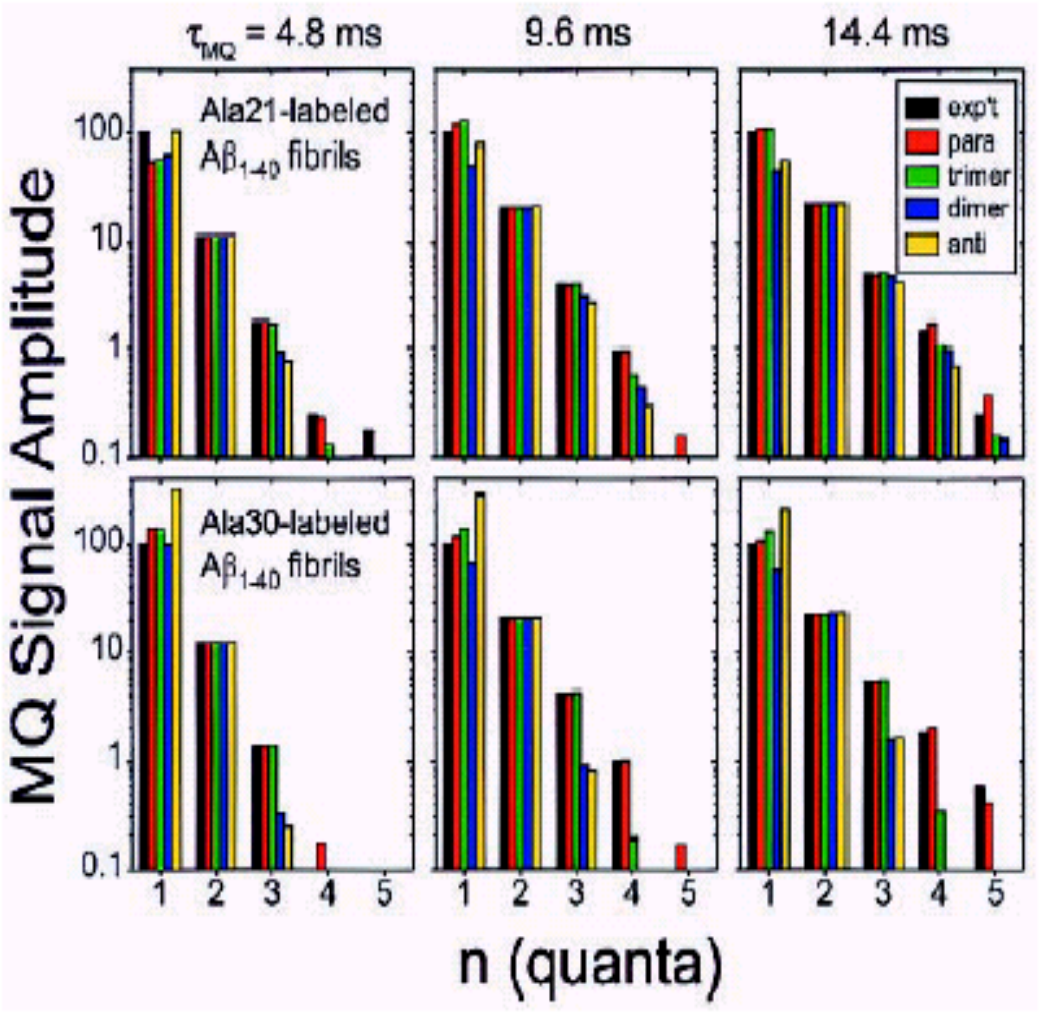

Fig. 3. Comparison of experimental MQNMR amplitudes (black) with simulations for parallel (red), trimeric (green), dimeric (blue), and antiparallel organizations of β-sheets in $A\beta_{1-40}$ fibrils, for samples labeled with ^{13}C at methyl carbons of Ala-21 and Ala-30. Experimental MQNMR amplitudes are normalized to a one-quantum amplitude of 100. A logarithmic vertical scale is required because the amplitudes vary over 2 orders of magnitude. The parallel β-sheet model fits all of the experimental data most closely. Experimental amplitudes were determined from MQNMR spectra in Fig. 2 by integrating each subspectrum over the interval from −2 kHz to +3 kHz. Uncertainties in the experimental amplitudes, evaluated as the rms noise integrated over a 5-kHz-wide interval, are ±0.11, ±0.14, and ±0.14 for the Ala-21-labeled $A\beta_{1-40}$ fibril data, and ±0.15, ±0.17, and ±0.24 for the Ala-30-labeled $A\beta_{1-40}$ fibril data, for τ_{MQ} = 4.8 ms, 9.6 ms, and 14.4 ms, respectively.

A structural model for Alzheimer's β-amyloid fibrils based on experimental constraints from solid state NMR

Aneta T. Petkova*, Yoshitaka Ishii*†, John J. Balbach*, Oleg N. Antzutkin‡, Richard D. Leapman§, Frank Delaglio*, and Robert Tycko*¶

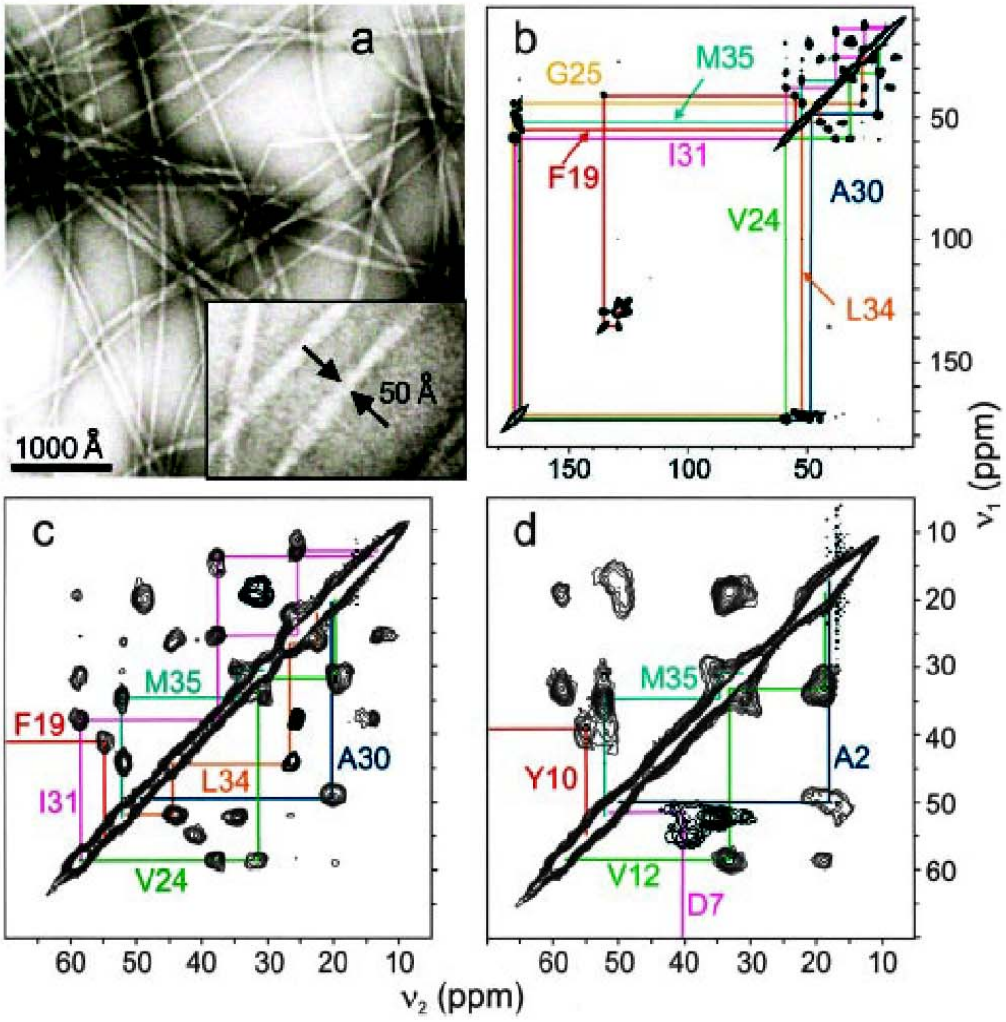

Fig. 1. (*a*) Transmission electron microscope images of negatively stained amyloid fibrils after 14-day incubation of a 0.5 mM $A\beta_{1-40}$ solution. A 3× expansion (*Inset*) shows fibrils with the smallest diameters observed. (*b*) 2D ^{13}C-^{13}C chemical shift correlation spectrum of $A\beta_{1-40}$ fibril sample SU7, showing resonance assignment paths for the seven uniformly ^{15}N- and ^{13}C-labeled residues in this sample. (*c*) Expansion of the aliphatic region of the 2D spectrum of SU7. (*d*) Aliphatic region of the 2D ^{13}C-^{13}C chemical shift correlation spectrum of $A\beta_{1-40}$ fibril sample SU6.

Table 1. ^{13}C and ^{15}N NMR chemical shift values (ppm) for ^{13}C- and ^{15}N-labeled sites in $A\beta_{1-40}$ fibrils, referenced to TMS (tetramethylsilane) or liquid NH_3

Residue	CO	C_α	C_β	C_γ	C_δ	C_κ	C_ζ, N_ζ	N	Sample
A2	173.7	49.9	18.2					ND	SU6
	(176.1)	(50.8)	(17.4)						
D7	~173.0	51.5	40.4	177.9				120.6	SU6
	(174.6)	(52.5)	(39.4)	(178.3)				(120.4)	
G9	169.3	42.9						107.2	SU6
	(173.2)	(43.4)						(108.8)	
Y10	172.0	55.0	39.5	126.5	130.7	116.5	156.2	122.4	SU6
	(174.2)	(56.2)	(37.1)	(128.9)	(131.6)	(116.5)	(155.6)	(120.3)	
V12	173.0	58.7	33.2	18.8, 18.8				127.0	SU6
	(174.6)	(60.5)	(31.2)	(19.4, 18.6)				(119.2)	
K16	171.5	52.7	34.1	24.0	28.6	39.8	33.7	ND	CU6
			36.9	24.8					
	(174.9)	(54.5)	(31.4)	(23.0)	(27.3)	(40.2)	(32.7)		
L17	172.8	52.3	~44.5	26.0	~24.4, ~23.3			ND	CU6
	173.0	51.6	~40.8	~27.0	~24.8, ~23.1				
	(175.9)	(53.4)	(40.7)	(25.2)	(23.2, 21.6)				
V18	170.3	58.9	33.6	19.2				121.7	CU6
	(174.6)	(60.5)	(31.2)	(19.4, 18.6)				(119.2)	
F19	170.2	55.3	41.0	135.7	129.6	129.6	125.8	130.5	CU6, SU7
	(174.1)	(56.0)	(37.9)	(137.2)	(130.2)	(129.8)	(128.2)	(120.3)	
F20	170.2	54.6	41.0	135.7	129.2	129.2	125.8	ND	CU6
	(174.1)	(56.0)	(37.9)	(137.2)	(130.2)	(129.8)	(128.2)		
A21	172.7	48.2	21.0					130.9	CU6
	174.0	48.0	18.9					126.3	
	(176.1)	(50.8)	(17.4)					(123.8)	
D23	173.1	51.0	41.9	180.2				118.5	SU5
	174.1	52.4	39.4	178.0				123.3	
	(174.6)	(52.5)	(39.4)	(178.3)				(120.4)	
V24	173.8	58.6	31.3	19.9, 18.3				125.0	SU7
	173.6	59.0	32.8	19.9, 19.9				125.0	
	(174.6)	(60.5)	(31.2)	(19.4, 18.6)				(119.2)	
G25	174.2	44.4						113.9	SU7
	171.1	46.9						117.8	
	171.1	~44.2						113.9	
	(173.2)	(43.4)						(108.8)	
K28	174.3	52.8	35.6	24.7	27.8	42.0	33.0	119.5	SU5
	172.4	53.5	33.4	22.3	28.5	39.1	32.9	112.7	
	(174.9)	(54.5)	(31.4)	(23.0)	(27.3)	(40.2)	(32.7)	(120.4)	
G29	172.4	47.2						117.0	SU5
	168.6	42.4						104.1	
	(173.2)	(43.4)						(108.8)	
A30	173.2	48.4	20.5					122.1	SU7
								127.4	
	171.3	49.5	20.5					119.2	
	(176.1)	(50.8)	(17.4)					(123.8)	
I31	172.5	58.4	38.0	25.7, 13.8	13.3			120.6	SU7
	(174.7)	(59.4)	(37.1)	(25.5, 15.7)	(11.2)			(119.9)	
I32	173.8	56.7	40.2	25.2, 15.9	12.4			125.0	SU5
	172.2	57.0	38.7	24.6, 15.3	12.1			125.0	
	(174.7)	(59.4)	(37.1)	(25.5, 15.7)	(11.2)			(119.9)	
L34	171.0	52.1	44.8	27.0	~24.0, 22.5			~128.0	SU7
			44.1	26.3	24.0, 22.9			~128.0	
	(175.9)	(53.4)	(40.7)	(25.2)	(23.2, 21.6)			(121.8)	
M35	171.2	52.1	34.6	30.8		16.7		125.4	SU7, SU6
	(174.6)	(53.7)	(31.2)	(30.3)		(15.2)		(119.6)	
V36	171.8	58.8	31.9	18.9				126.6	SU5
	(174.6)	(60.5)	(31.2)	(19.4, 18.6)				(119.2)	

Values preceded by ~ have an uncertainty of 0.6 ppm. Otherwise, the uncertainty is 0.3 ppm. Values that could not be determined are indicated by ND. Values in parentheses are random-coil shifts, taken from Wishart *et al.* (51) and adjusted to the TMS reference.

TABLE IX

CHEMICAL SHIFT VALUES FOR BACKBONE ATOMS USED IN DETERMINATION OF SECONDARY STRUCTURE[a]

Residue	α-^{1}H range	2-^{13}C range	1-^{13}C range
Ala	4.35 ± 0.10	52.2 (+0.8, −0.5)	177.6 ± 0.5
Cys	4.65 ± 0.10	56.8 (+0.8, −0.5)	174.1 ± 0.5
Asp	4.76 ± 0.10	53.9 (+0.8, −0.5)	176.8 ± 0.5
Glu	4.29 ± 0.10	56.5 (+0.8, −0.5)	176.6 ± 0.5
Phe	4.66 ± 0.10	57.9 (+0.8, −0.5)	175.5 ± 0.5
Gly	3.97 ± 0.10	45.0 (+0.8, −0.5)	173.6 ± 0.5
His	4.63 ± 0.10	55.5 (+0.8, −0.5)	174.9 ± 0.5
Ile	3.95 ± 0.10	61.2 (+0.8, −0.5)	176.5 ± 0.5
Lys	4.36 ± 0.10	56.5 (+0.8, −0.5)	176.5 ± 0.5
Leu	4.17 ± 0.10	55.0 (+0.8, −0.5)	176.9 ± 0.5
Met	4.52 ± 0.10	55.2 (+0.8, −0.5)	177.0 ± 0.5
Asn	4.75 ± 0.10	52.7 (+0.8, −0.5)	175.6 ± 0.5
Pro	4.44 ± 0.10	63.0 (+0.8, −0.5)	176.0 ± 0.5
Gln	4.37 ± 0.10	56.0 (+0.8, −0.5)	175.6 ± 0.5
Arg	4.38 ± 0.10	56.0 (+0.8, −0.5)	176.6 ± 0.5
Ser	4.50 ± 0.10	58.1 (+0.8, −0.5)	174.7 ± 0.5
Thr	4.35 ± 0.10	62.0 (+0.8, −0.5)	175.5 ± 0.5
Val	3.95 ± 0.10	62.2 (+0.8, −0.5)	176.0 ± 0.5
Trp	4.70 ± 0.10	57.6 (+0.8, −0.5)	175.6 ± 0.5
Tyr	4.60 ± 0.10	58.0 (+0.8, −0.5)	175.9 ± 0.5

[a] Data are given in ppm, relative to DSS.

Structural information deduced from solid state NMR spectroscopy

- Secondary shifts are strongly correlated with peptide or protein backbone conformation. In particular, values for β-strand segments are characteristically negative for $^{13}C_{\alpha}$ and ^{13}CO sites and positive for $^{13}C_{\beta}$ sites.

- Multiplicity of chemical shifts was attributed to the differences in molecular structure associated with the differences in fibril morphology.

- ^{13}C chemical shifts for D23, V24, G25 and G29 are inconsistent with expectations for a β-strand. Thus, the chemical shift data qualitatively suggest a conformation for the structurally ordered part of $A_{\beta 1\text{-}40}$ consisting of two β-strands that are separated by a bend or loop contained within residues 23-29. The conformation in the bend segment may vary with fibril morphology and fibrillization conditions.

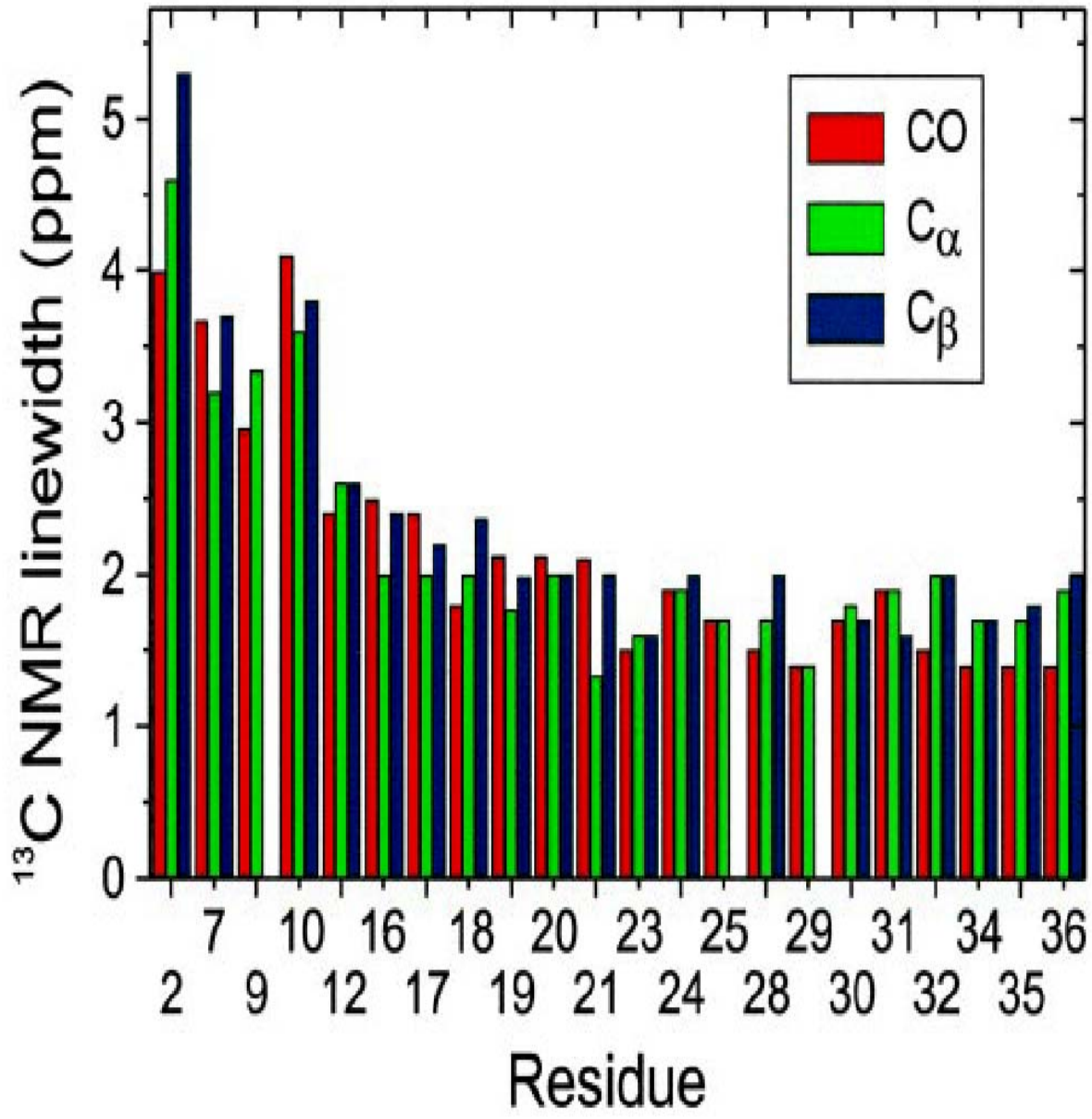

Fig. 2. ^{13}C NMR linewidths for CO, Cα, and Cβ sites in Aβ_{1-40} fibrils, determined from 2D solid state NMR spectra as in Fig. 1. Linewidths of 2.5 ppm or less indicate well-ordered conformations. Larger linewidths in the N-terminal segment indicate structural disorder.

Structural information deduced from solid state NMR spectroscopy

- Secondary shifts $\Delta\delta \equiv \delta_{fibril} - \delta_{coil}$ are strongly correlated with peptide or protein backbone conformation. In particular, values for β-strand segments are characteristically negative for $^{13}C_{\alpha}$ and ^{13}CO sites and positive for $^{13}C_{\beta}$ sites.

- Multiplicity of chemical shifts was attributed to the differences in molecular structure associated with the differences in fibril morphology.

- ^{13}C chemical shifts for D23, V24, G25 and G29 are inconsistent with expectations for a β-strand. Thus, the chemical shift data qualitatively suggest a conformation for the structurally ordered part of $A_{\beta 1\text{-}40}$ consisting of two β-strands that are separated by a bend or loop contained within residues 23-29. The conformation in the bend segment may vary with fibril morphology and fibrillization conditions.

- Linewidths in the 1.5-2.5 ppm range in solid state ^{13}C MAS NMR spectra are characteristic of well-structured peptide in rigid noncrystalline environments, whereas significantly larger linewidths are observed in disordered biopolymers shows that the N-terminal segment of $A_{\beta 1\text{-}40}$ is disordered in the fibrils.

Table 2. Residue-specific ϕ and ψ backbone torsion angles (degrees) for Aβ_{1-40} fibrils, predicted from ^{13}C and ^{15}N chemical shifts in Table 1 or determined from measurements on the doubly ^{13}C-labeled DLn samples

Residue	ϕ, ψ from chemical shift set 1*	ϕ, ψ from chemical shift set 2†	ϕ, ψ from DLn samples
G9	−148 ± 11, 151 ± 15	−148 ± 11, 151 ± 15	
Y10	−127 ± 9, 124 ± 9	−127 ± 9, 124 ± 9	
V12	−119 ± 8, 124 ± 10	−119 ± 8, 124 ± 10	
K16	−149 ± 12, 152 ± 8	−149 ± 12, 152 ± 8	
L17	−150 ± 12, 143 ± 9	−150 ± 12, 143 ± 9	
V18	−145 ± 9, 147 ± 11	−145 ± 8, 146 ± 12	
F19	−144 ± 10, 141 ± 12	−144 ± 10, 139 ± 15	
F20	−147 ± 9, 151 ± 11	−145 ± 11, 152 ± 13	
A21	−137 ± 12, 143 ± 16	−127 ± 11, 141 ± 19	
D23	−145 ± 16, 147 ± 16	−83 ± 13, 122 ± 22	
V24	−103 ± 10, 117 ± 11	−100 ± 12, 114 ± 22	−145, 115
G25	−88 ± 30, 124 ± 33	−58 ± 48, 11 ± 74	−70, −40
S26			68, −65
K28	−134 ± 12, 152 ± 14	−151 ± 14, 156 ± 13	
G29	−59 ± 50, 119 ± 58	−150 ± 18, 156 ± 14	−120, −125
A30	−138 ± 14, 157 ± 14	−144 ± 12, 145 ± 13	−165, 133
I31	−113 ± 16, 127 ± 12	−118 ± 15, 129 ± 11	
I32	−123 ± 10, 146 ± 14	−127 ± 9, 147 ± 12	
L34	−143 ± 9, 145 ± 17	−144 ± 8, 145 ± 16	
M35	−141 ± 9, 138 ± 11	−141 ± 9, 138 ± 11	
V36	−118 ± 8, 120 ± 11	−118 ± 8, 120 ± 11	

*First chemical shift value for each labeled site in Table 1.

†Second chemical shift value for each labeled site in Table 1, where more than one value is observed.

(c) Distance d_{NN} and torsion angles relationship – Ramachandran plot

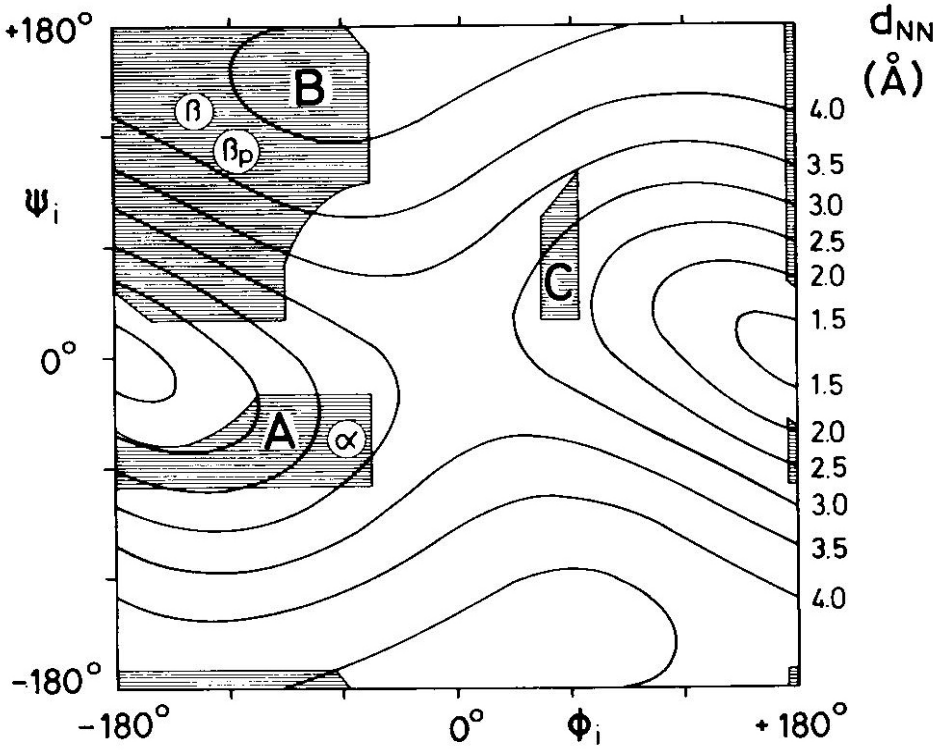

Figure 7.7. Sequential distance d_{NN} in the ϕ_i–ψ_i plane; solid contour lines represent fixed values of d_{NN} as indicated on the right. The shaded areas A, B, and C are sterically allowed for an alanyl dipeptide (Ramachandran and Sasisekharan, 1968). α, β, and β_p indicate the ϕ_i–ψ_i combinations for the regular α helix, antiparallel β sheet, and parallel β sheet (from Billeter et al., 1982).

Structural information deduced from solid state NMR spectroscopy

- Secondary shifts $\Delta\delta \equiv \delta_{fibril} - \delta_{coil}$ are strongly correlated with peptide or protein backbone conformation. In particular, values for β-strand segments are characteristically negative for $^{13}C_{\alpha}$ and ^{13}CO sites and positive for $^{13}C_{\beta}$ sites.

- Multiplicity of chemical shifts was attributed to the differences in molecular structure associated with the differences in fibril morphology.

- ^{13}C chemical shifts for D23, V24, G25 and G29 are inconsistent with expectations for a β-strand. Thus, the chemical shift data qualitatively suggest a conformation for the structurally ordered part of $A_{\beta 1\text{-}40}$ consisting of two β-strands that are separated by a bend or loop contained within residues 23-29. The conformation in the bend segment may vary with fibril morphology and fibrillization conditions.

- Linewidths in the 1.5-2.5 ppm range in solid state ^{13}C MAS NMR spectra are characteristic of well-structured peptide in rigid noncrystalline environments, whereas significantly larger linewidths are observed in disordered biopolymers shows that the N-terminal segment of $A_{\beta 1\text{-}40}$ is disordered in the fibrils.

- ^{13}C chemical shifts for CO, C_{α} and C_{β} sites and ^{15}N chemical shifts for backbone amide were analyzed to predict the backbone torsion angles for each residue. Predictions for two different choices of chemical shifts values are derived. Both lead to $\phi = -135^{\circ} \pm 25^{\circ}$ and $\psi = 140^{\circ} \pm 20^{\circ}$, consistent with a β-strand conformation, for all residues in the 9-21 and 30-36 segments. Non-β-strand ϕ and ψ values occur at D23, G25 and G29.

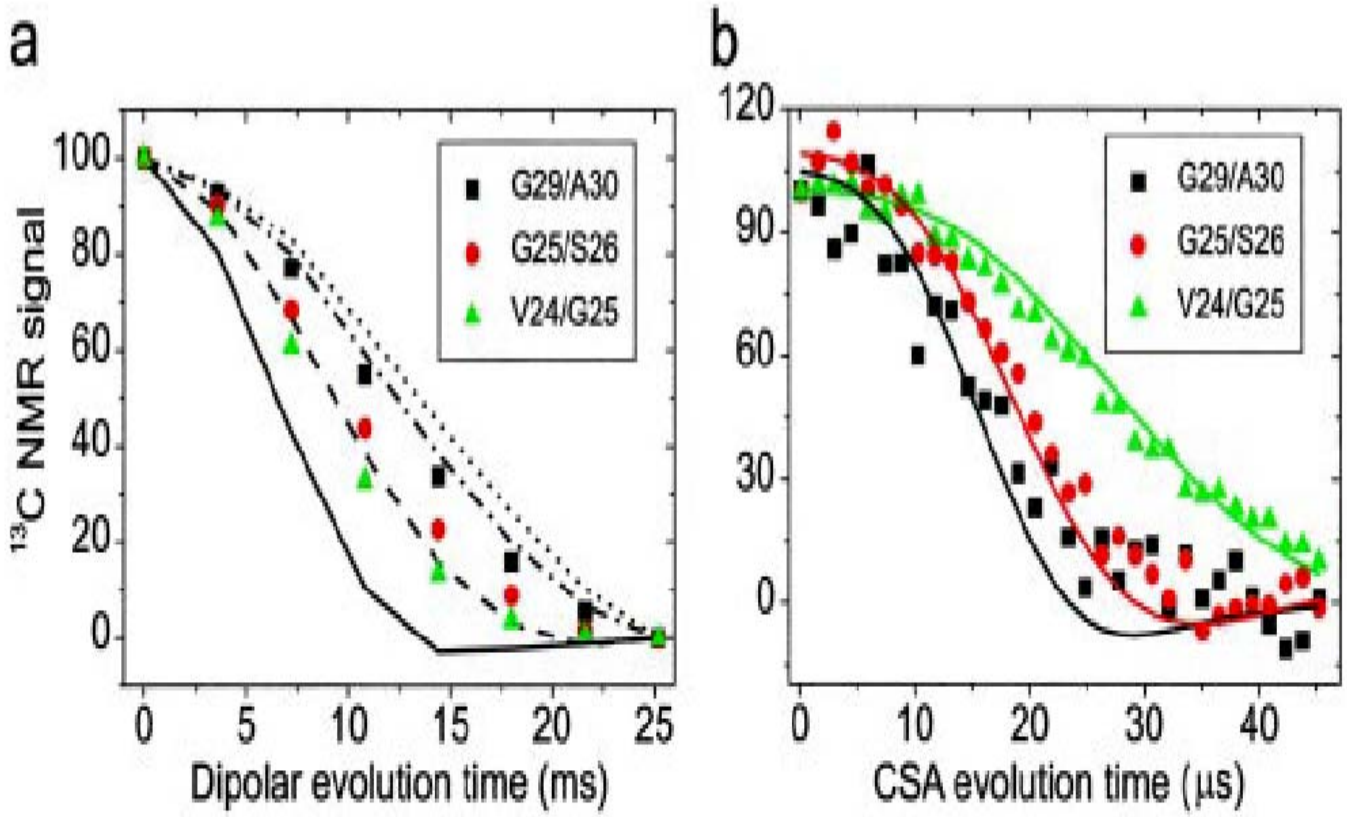

Fig. 3. Solid state NMR data on DLn Aβ_{1-40} fibril samples with ^{13}C labels at the indicated backbone carbonyl sites. These data constrain the ϕ and ψ angles of the second labeled residue. (*a*) fpRFDR-CT data and simulations for $\phi = 40°$ (solid line), 80° (dashed line), 120° (dot-dashed line), and 160° (dotted line). Simulations are scaled and baseline-corrected to match the first and last experimental data points. (*b*) DQCSA data and simulations for ϕ, $\psi = -70°$, $-40°$ (green); 70°, $-65°$ (red); and $-165°$, 135° (black).

Structural information deduced from solid state NMR spectroscopy

- Linewidths in the 1.5-2.5 ppm range in solid state ^{13}C MAS NMR spectra are characteristic of well-structured peptide in rigid noncrystalline environments, whereas significantly larger linewidths are observed in disordered biopolymers shows that the N-terminal segment of $A_{\beta 1\text{-}40}$ is disordered in the fibrils.

- ^{13}C chemical shifts for CO, C_α and C_β sites and ^{15}N chemical shifts for backbone amide were analyzed to predict the backbone torsion angles for each residue. Predictions for two different choices of chemical shifts values are derived. Both lead to $\phi = -135^\circ \pm 25^\circ$ and $\psi = 140^\circ \pm 20^\circ$, consistent with a β-strand conformation, for all residues in the 9-21 and 30-36 segments. Non-β-strand ϕ and ψ values occur at D23, G25 and G29.

- In RFDR-CT measurements, the decay of ^{13}C NMR signals from the labeled carbonyl sites reflects the strength of ^{13}C-^{13}C dipole-dipole couplings, which depends primarily on the intramolecular ^{13}C-^{13}C distance and hence the ϕ angle. In DQCSA measurements, the decay of ^{13}C NMR signals from the labeled sites reflects the relative orientation of the labeled carbonyl groups, which depends on both ϕ and ψ. The RFDR-CT and DQCSA data for different samples are significantly different, indicating significant differences in . Qualitatively, this result indicates the presence of non-β-strand conformations.

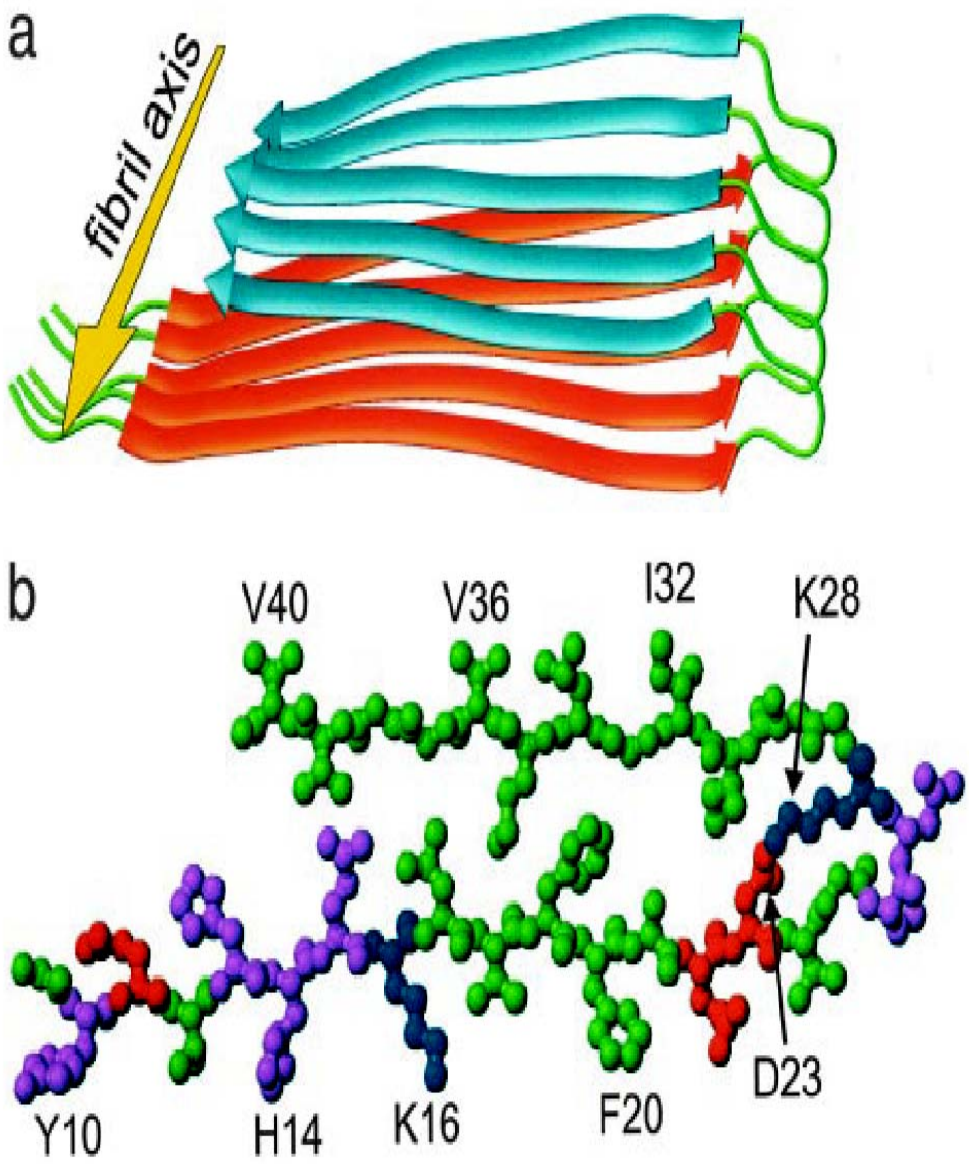

Fig. 4. Structural model for $A\beta_{1-40}$ fibrils, consistent with solid state NMR constraints on the molecular conformation and intermolecular distances and incorporating the cross-β motif common to all amyloid fibrils. Residues 1–8 are considered fully disordered and are omitted. (*a*) Schematic representation of a single molecular layer, or cross-β unit. The yellow arrow indicates the direction of the long axis of the fibril, which coincides with the direction of intermolecular backbone hydrogen bonds. The cross-β unit is a double-layered structure, with in-register parallel β-sheets formed by residues 12–24 (orange ribbons) and 30–40 (blue ribbons). (*b*) Central $A\beta_{1-40}$ molecule from the energy-minimized, five-chain system, viewed down the long axis of the fibril. Residues are color-coded according to their sidechains as hydrophobic (green), polar (magenta), positive (blue), or negative (red).

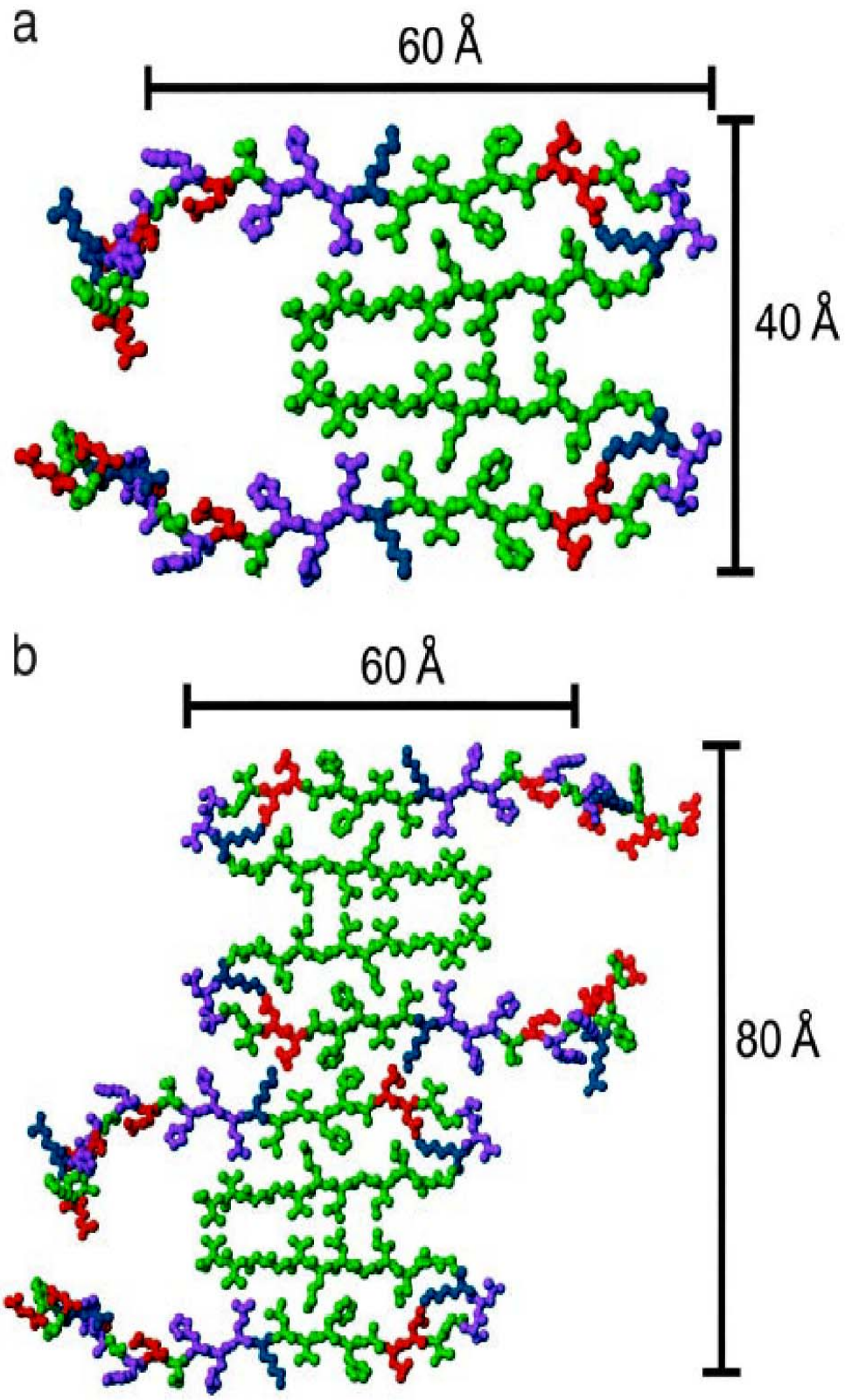

Fig. 5. (*a*) Cross section of an Aβ_{1-40} fibril with the minimal MPL indicated by scanning transmission electron microscopy (13, 29), formed by juxtaposing the hydrophobic faces of two cross-β units from Fig. 4. Residues 1–8 are included with randomly assigned conformations. (*b*) Possible mode of lateral association to generate fibrils with greater MPL and greater cross-sectional dimensions.